Programmed knockout mutation of liver fluke granulin, *Ov-grn-1*, attenuates virulence and impedes malignant transformation during chronic opisthorchiasis

Sujittra Chaiyadet[1, 2, 3] Sirikachorn Tangkawattana[3,4], Michael J Smout[3,5,], Wannaporn Ittiprasert[3,6], Victoria H. Mann[6], Raksawan Deenonpoe[7], Patpicha Arunsan[1,6], Alex Loukas[5,8], Paul J Brindley[6, 8], Thewarach Laha[1,8]

[1] Department of Parasitology, Faculty of Medicine, Khon Kaen University, Khon Kaen, 40002 Thailand

[2] Tropical Medicine Graduate Program, Academic Affairs, Department of Parasitology, Faculty of Medicine, Khon Kaen University, Khon Kaen, 40002 Thailand

[3]equal contribution

[4] Faculty of Veterinary Medicine, Khon Kaen University, Khon Kaen, Thailand, and WHO Collaborating Center for Research and Control of Opisthorchiasis, Tropical Disease Research Center, Khon Kaen University, Khon Kaen 40002, Thailand

[5] Centre for Molecular Therapeutics, Australian Institute of Tropical Health and Medicine, James Cook University, Cairns, Queensland, 4878, Australia

[6] Department of Microbiology, Immunology and Tropical Medicine, and Research Center for Neglected Diseases of Poverty, School of Medicine & Health Sciences, George Washington University, Washington, D.C. 20037, USA

[7]Department of Pathology, Faculty of Medicine, Khon Kaen University, Khon Kaen, 40002 Thailand

[8]correspondence: Thewarach Laha, email, thewa_la@kku.ac.th; Alex Loukas, email, alex.loukas@jcu.edu.au; Paul Brindley, email, pbrindley@gwu.edu

Abstract

Infection with the food-borne liver fluke *Opisthorchis viverrini* is the principal risk factor for cholangiocarcinoma (CCA; bile duct cancer) in the Lower Mekong River Basin countries including Thailand, Lao PDR, Vietnam, Myanmar and Cambodia. Using gene edited liver flukes in a hamster model of CCA involving concurrent infection and administration of sub-carcinogenic levels of nitrosamine, we explored the role of the fluke granulin-like growth factor *Ov*-GRN-1 in malignancy. We produced programmed gene knockout flukes (*ΔOv-grn-1)* by delivery of a CRISPR/Cas9/gRNA system by square wave electroporation. Targeted genome sequencing confirmed Cas9-catalyzed mutations in target parasite genes, and the rapid depletion of transcripts and the targeted proteins. Hamsters were infected with gene edited larval parasites and exposed to sub-carcinogenic levels of dimethyl nitrosamine in drinking water. Whereas *Ov-grn-1* gene-edited parasites colonized the biliary tract of hamsters and developed into adult flukes, less hepatobiliary tract disease manifested during chronic infection with *ΔOv-grn-1* worms in comparison to hamsters infected with control parasites. Specifically, immunohistochemical analysis of thin sections of hamster livers revealed markedly less fibrosis surrounding flukes and less global liver fibrosis as a result of infection with *ΔOv-grn-1* worms, minimal biliary epithelial cell proliferation, and markedly fewer mutations of *TP53* in biliary epithelial cells. Moreover, fewer hamsters developed high grade CCA when infected with *ΔOv-grn-1* flukes compared to controls. The clinically-relevant pathophysiological phenotype of the livers of the hamsters confirmed a role for this parasite secreted growth factor in morbidity and malignancy during opisthorchiasis.

Keywords

Infection-associated cancer; liver fluke; opisthorchiasis; cholangiocarcinoma; CRISPR/Cas; knockout; granulin

Introduction

Liver fluke infection caused by species of *Opisthorchis* remains a major public health problem in East Asia and Eastern Europe. Infection with *O. viverrini* is endemic in Thailand and Laos, where ~10 million people are infected with the parasite. Opisthorchiasis is associated with hepatobiliary diseases including cholangiocarcinoma (Kitadokoro et al.), or bile duct cancer (Brindley et al., 2021). Northeast Thailand reports the world's highest incidence of CCA, >80 per 100,000 in some provinces. No stronger link between malignancy and a parasitic infection occurs than that between CCA and *O. viverrini.* Indeed, the International Agency for Research on Cancer of the World Health Organization classifies infection with *O. viverrini* as a Group 1 carcinogen, i.e. definitely carcinogenic in humans (Brindley *et al.*, 2021; Brindley et al., 2015; IARC, 2012).

The mechanism by which opisthorchiasis induces CCA is likely multi-factorial, including mechanical irritation of the biliary tract during migration and feeding of the liver fluke, metabolites released by the parasite, and nitrosamines in fermented foods that are a dietary staple in countries of the Mekong River basin. To survive in hostile environs, parasitic helminths excrete and secrete a battery of proteins (excretory/secretory proteins [ES]) and other mediators with diverse effects and roles at the host–parasite interface. This interaction has long been thought to manipulate host cellular homeostasis and underwrite malignant transformation during chronic opisthorchiasis, but the molecular mechanisms by which these processes occur are poorly understood. Focusing on the ES contribution to carcinogenesis, we here targeted the growth factor *Ov*-GRN-1, *O. viverrini* granulin, one component of the ES complement that we have determined induces phenotypic hallmarks of cancer (Smout et al., 2009). We have reported that *Ov*-GRN-1 and other ES components including extracellular vesicles (EVs) enter cholangiocytes, the epithelial cells that line the biliary tract, and drive cellular signaling that can promote carcinogenesis, including cellular proliferation and migration, angiogenesis and wound healing (Chaiyadet et al., 2015). Also, we recently confirmed the role of *Ov*-GRN-1 in driving proliferation of bile duct epithelial cells (cholangiocytes) by genetic manipulation of its expression in the liver fluke both by RNAi and by CRISPR/Cas9 gene editing (Arunsan et al., 2019). Moreover, we have shown that infection of hamsters with gene edited infectious fluke

larvae is feasible and, shown that proliferation of biliary epithelia is markedly suppressed during infection with the *Ov-grn-1-/-* (*ΔOv-grn-1*) flukes.

There is an established, tractable model of induction of CCA in experimentally infected hamsters, where 100% of hamsters infected with metacercariae of the parasite and exposed to otherwise sub-carcinogenic levels of dietary dimethyl nitrosamine (DMN) develop CCA within a few months after infection with the liver fluke (Loilome et al., 2006; Thamavit et al., 1987; Thamavit et al., 1994). In the Syrian golden hamster, *O. viverrini* infection causes periductal fibrosis. Severe periductal fibrosis induced by the parasite combined with a nitric oxide carcinogen, such as DMN, results in epithelial hyperplasia, cholangiocyte proliferation and DNA damage, eventually culminating in CCA in hamsters (Sripa et al., 2007). Here, we investigated the effect of infection of hamsters with *O. viverrini* following programmed knock out the *Ov-grn-1* gene in the infective stage of the liver fluke before experimental infection of hamsters in relation to fluke induced periductal fibrosis and malignant transformation of the hepatobiliary tract. Immunohistochemical analysis of thin sections of hamster livers revealed markedly less fibrosis during infection with *ΔOv-grn-1* worms, minimal cholangiocyte proliferation, substantially less expression of mutant p53 tumor protein, and diminished malignancy of the hepatobiliary tract. The clinically-relevant, pathophysiological phenotype of the livers of the hamsters confirmed a role for this parasite secreted growth factor in morbidity and malignancy during opisthorchiasis, and highlight the tractability of CRISPR-Cas9 for addressing gene function in flatworms.

Results

Programmed CRISPR/Cas-9 knock-out of genes of *O. viverrini*

To investigate the effect of programmed gene knock-out in *O. viverrini*, hamsters were infected with NEJs of *O. viverrini* that had been subjected to CRISPR/Cas genome editing. The C CRISPR/Cas systems were delivered by electroporation of plasmids encoding guide RNAs specific for *Ov-grn-1* or *Ov-tsp-2* or a control (scramble - SCR) guide RNA and Cas9 of *S.*

pyogenes. Figure 1A summarizes the experimental approach and timelines, findings from which are detailed below.

Changes in transcription of the targeted genes that would reflect programmed genomic changes were monitored by RT-qPCR. Relative to the SCR group, the *Ov-grn-1* transcript levels were significantly reduced in the *ΔOv-grn-1* flukes by 37.6% ($P<0.05$) whereas the transcription of *Ov-tsp-2* was not significantly changed in the *ΔOv-grn-1* flukes (18%, *ns*) (Figure 1B). Transcription of *Ov-tsp-2* was significantly reduced in the *ΔOv-tsp-2* flukes (62.1%; $P<0.01$) whereas the levels of *Ov-grn-1* transcripts were not significantly changed (Figure 1C). These findings indicated on-target gene knockout at both the *Ov-grn-1* and *Ov-tsp-2* loci.

Effect of CRISPR/Cas-9 targeted mutation of *Ov-grn-1* or *Ov-tsp-2* on adult flukes

In experiment 1, feces were sampled from each hamster at both 10 and 12 weeks after infection. Significant differences in fecal eggs (EPG) were not apparent among the three groups at these timepoints (Figure 2A). Hamsters were euthanized and necropsied at 14 weeks to investigate the numbers of adult *O. viverrini* in the hepatobiliary tract. The numbers of worms in the control SCR, *ΔOv-grn-1*, and *ΔOv-tsp*-2 groups were 60.0±3.46 (mean ± SEM), 36.7±3.48, and 21.3±2.96, reflecting reductions of 38.9% and 64.5%, respectively, compared to the SCR control group (Figure 2B).

Of the worms recovered from the livers, 10-13 from each of the three hamsters in each group were evaluated by RT qPCR for gene transcript levels relative to the SRC (control) flukes. Transcipt levels of both genes expressed by the control SCR parasites were generally clustered around 100% (Figure 2C, D). Transcript levels for *Ov-grn-1* ranged broadly in the Δ*Ov-grn-1* flukes but were significantly reduced by 54% compared to the SCR group (Figure 2C; $P\leq 0.001$). This broad range, 100 – 0%, in *Ov-grn-1* transcript levels was similar to the findings in our earlier report (Arunsan *et al.*, 2019). The outcome, where most flukes either not showing a change (~100%) or, by contrast, showing a near absence of transcription (~0%) was not normally distributed, which required a non-parametric statistical approach. Median values were reported for these analyses. In contrast to the NEJ, which showed substantial knockdown of *Ov-tsp*-2

(Figure 1), the adult stage *ΔOv-tsp*-2 flukes showed only a modest reduction in transcript levels (9%) compared to the SCR group (Figure 2D). Although the *Ov-tsp*-2 transcript levels were significantly reduced ($P \leq 0.01$), the transcript levels mostly showed minimal change and only two individual flukes exhibited > 50% reduction in expression. This marked difference, when compared to transcript levels in NEJ (reduced by 62.1%), in addition to the reduction by 65% of numbers of worms recovered at necropsy, indicated that *Ov-tsp-2* gene knockout |was a lethal phenotype and that flukes of this genotype failed to survive *in vivo*. This contrasted with programmed knockout of *Ov-grn-1* where the majority of Δ*Ov-grn-1* flukes survived even though transcription of *Ov-grn-1* was not detected in four of 36 flukes and 10 of 36 exhibited *Ov-grn-1* transcript levels <5% of those expressed in the SRC worms.

Parasitological impact of CRISPR/Cas-9 gene knockout

A primary goal for experiment 2 was the histopathological and histochemical assessment of hepatobiliary disease at 24 weeks of infection. Accordingly, determining the number of surviving liver flukes was not feasible because the liver and its intrahepatic biliary tract, occupied by the parasites, was fixed in formalin at necropsy. However, a sample of the resident *O. viverrini* were collected, to screen for efficacy of CRISPR/Cas9 gene knockout, before formalin fixation of the the liver. In lieu of counting the number of worms parasitizing each hamster, fecal egg count (as eggs per gram of feces, EPG) were determined at the time of necropsy. Numbers of eggs of *O. viverrini* positively correlate with number of worms within the hepatobiliary tract (Elkins et al., 1991; Kim et al., 2011). There was a broad range of EPG values among all three groups (Figure 3A) although feces of the SCR fluke infected hamsters had the highest EPG values, median =11,062 EPG, the *ΔOv-grn-1* group, 5,267 EPG, and the *ΔOv-tsp-2* group 4,530 EPG ($P \leq 0.05$), reflecting the same rank order in numbers of worms recovered from these three groups in experiment 1 (Fig. 2B). Although the number of fecal eggs correlates positively with numbers of worms during infection with *O. viverrini* (Elkins *et al.*, 1991), the variations in numbers of flukes among the groups, as predicted from the EPG values, confounds comparisons of the corresponding pathogenesis and lesions. Hence, to mitigate the impact of variations in numbers of liver flukes on the analysis and interpretation of the role of gene knockout on hepatobiliary disease and malignancy, the histopathological assessments focused on the livers of hamsters with

"moderate" EPG values, i.e. *ΔOv-grn-1* EPG ranging from 1,000 to 20,000 (Figure 3A, B, dotted lines). This cutoff window excluded three SCR hamsters with values of 26,000 to 44,000 EPG and four *ΔOv-tsp*-2-infected hamsters with ≤ 1,000 EPG. Figure 3B shows the "moderate EPG" values with 9,279 EPG in SCR-, 5,267 in Δ*Ov-grn-1*- and 5,434 in *ΔOv-tsp-2*-fluke infected hamsters with overlapping inter-quartile ranges. Significant differences among the groups (within the cutoff window) were not apparent. Whereas the surviving flukes did not show changes in expression of *Ov-tsp*-2 (Figures 2D and 3D), the hamsters infected with *ΔOv-tsp*-2 parasites were included as a low fluke burden comparator. It was likely that fewer flukes survived in the *ΔOv-tsp*-2 group of hamsters, including those hamsters with comparable EPGs, (Figure 2A, B).

Adult worms recovered from hamster livers examined at 24 weeks after infection were evaluated for targeted gene transcripts by qPCR. Transcript levels of *Ov-grn-1* in adult *O. viverrini* from Δ*Ov-grn-1* infected hamsters were significantly decreased (89%, $P \leq 0.0001$) compared to the SCR control group (Figure 3C), whereas the *ΔOv-tsp-2* flukes showed a non-significant increase (8%) compared to the SCR group (Figure 3D). With experiments 1 and 2 showing the surviving *ΔOv-tsp-2* worms expressing *Ov-tsp-2* at levels comparable to the control SCR flukes, we posit that substantial *Ov-tsp-2* gene edits were lethal, and worms that survived to maturity likely had not undergone gene editing and/or few of the cells in the worms had been edited. Although we retained the *ΔOv-tsp-2* group for comparison of pathogenesis, the genotype of the flukes from this group was not investigated further by targeted amplicon NGS.

Synopsis of outcomes of CRISPR/Cas9 gene editing of the liver flukes

To characterize mutations from the programmed knockouts, a region of 173 bp region flanking the programmed cleavage site in *Ov-grn-1* was investigated by analyzing reads from targeted amplicon NGS and analysis of the reads with CRISPresso2 (Clement et al., 2019). Substitution patterns as determined by the CRISPR-sub tool (Hwang et al., 2020a) in reads in the knockout groups were not significantly different from the cognate alleles in the control SCR group worms (Figure S1). Also, we scanned insertions and deletions (indels) and, in turn, the potential impact of indels on the open reading frame. Figure 4A and Table S1 present the indel percentages of

NEJs and adult flukes. The Δ*Ov-grn-1* pooled NEJs showed 3.26% indel levels (2,723 of 80,571 reads), significantly more than the 0.035% level in the SCR NEJ group (18 of 51,402 reads) ($P \leq 0.05$). The NEJ and SCR adult flukes showed a similar indel % levels, with 0.045% in the adults (41 of 91,783 reads). Thirteen individual Δ*Ov-grn-1* adult liver flukes displayed a broad range of editing efficiency in terms of indel profiles. These ranged from an apparent absence of programmed mutation (no indels) to near complete gene knockout (91% indels), with a median of 3.1% ($_{M}$Δ*Ov-grn-1*), which was significantly higher than in the SCR group flukes ($P \leq 0.01$). As noted for levels of transcription, however, there were apparently distinct groupings of low mutation flukes, six worms, (termed $_{L}$Δ*Ov-grn-1*) and six high mutation flukes ($_{H}$Δ*Ov-grn-1*) observed. From a total of ~1.5 million NGS reads, programmed deletions (~0.5 million) were overwhelmingly more common than insertions, seven of which seven were identified (Table S1).

The Δ*Ov-grn-1* indel percentage showed a strong inverse correlation with the transcript level (Figure 4B), with a two-tailed non-parametric Spearman correlation co-efficient $r_s = -0.74$ ($P \leq 0.01$). The highly mutated, $_{H}$Δ*Ov-grn-1* flukes only minimally expressed the targeted *Ov-grn-1* gene, <11% level of transcription of control SRC liver flukes. However, the highly edited genotype/highly reduced transcription phenotype contrasted with the wide range of transcription in the flukes with low or moderate levels of editing, $_{L}$Δ*Ov-grn-1* and $_{M}$Δ*Ov-grn-1*, with a wide range of transcription from 6% to 94% of the levels of the control SRC group worms.

Evaluation of nucleotide position of indels

With respect to indel length and position, mutations were spread 29 bp upstream and 54 bp downstream of the double stranded break (DSB+ (ORF nucleotide position -10 to +74). Most indels were deletions of a single nucleotide, some were as long as four nt and the longest was 62 nt. Deletions were noted along the length of the amplicon, with several higher frequency sites indicated with bubbles of greater diameter in Figure 4C. The pooled NEJ indel locations reflected the high frequency adult locations (Figure 4C, large bubbles). As noted, insertions were infrequently seen but they tended to associate around these high frequency indel locations in NEJs and adult flukes. Of note was the mutation cluster at -1 to -10 bp, within the 5' untranslated region (UTR) of the ORF. Of the 216 indels observed in adult flukes, 48 (22%)

occurred in this region, and five specific sites included indels from 7 or more adult worms. Figure 4D shows the frequency within each sample at each base pair position. Notably, there were hotspot locations in the ORF at which both SCR and Δ*Ov-grn-1* NEJs and adults all showed a mutation, albeit at low frequency. All four ACGT nucleotides were represented in the hotspots. Whereas these hotspots occurred across all groups, they were infrequently seen, with the most common ORF hotspot seen at position 9T in ~0.02% of the genomes sequenced. The 5'UTR cluster at nt position -1 to -10 was also a distinct grouping of mutations in this panel, with no mutations at this location in SCR flukes and only a single $_{L}$Δ*Ov-grn-1* minimally edited fluke in this 10 bp segment. While the cluster was of interest, the striking feature was the highly mutated -9T position. This single position comprised ~99% of the total indel% for $_{M/H}$*ΔOv-grn-1* flukes and *ΔOv-grn-1* NEJs. Despite this single position being highly mutated and the neighboring base pairs comprising the commonly *ΔOv-grn-1* mutated cluster, the next highest frequency position was -8C with only a small proportion of mutated cells recorded (<0.09%).

Programmed knockout of *Ov-grn-1* impeded malignant transformation

The CCA hamster model employed, concurrent liver fluke infection and exposure to DMN (Thamavit *et al*., 1987), induced malignant transformation by the 24 week end point of experiment 2. Predominant lesions of various types were common in all groups, and the high grade CCA whole liver images highlight the most severe pathogenesis from the 24 week infection (Figure 5A, B). Liver pathogenesis such as the pre-cancerous dysplasia stage were evident in many bile duct epithelia and usually surrounded by fibrosis (Figure 5C). Representative micrographs of the high grade cancerous transformation from the three groups are shown in Figure 5D-F. Figure 5G and Table S2 summarize the pathology findings in the three groups of hamsters. Ten of 12 (83.3%) hamsters in the control SCR group were diagnosed with CCA, with high grade CCA in eight of the 10 hamsters and low grade CCA in other two. Dysplasia, a precancerous lesion of CCA (Shimonishi et al., 2000) was diagnosed in the remaining two of the 12 (one mild, one moderate) hamsters in the SCR group. CCA emerged in seven of 13 hamsters (six with high grade CCA) in the Δ*Ov-tsp-2* group. Of the remaining hamsters, mild dysplasia was seen in two, proliferation in one, inflammation in two, and the final hamster was free of hepatobiliary lesions. CAA was diagnosed in nine of 13 in the *ΔOv-grn-1*

group, four with high grade CCA. Of the remaining hamsters, one showed moderate dysplasia, two showed proliferation, and one was free of hepatobiliary lesions. Lesions less severe than dysplasia, i.e. inflammation, proliferation, or no lesions, were evident in several hamsters infected with Δ*Ov-tsp-2* (4/13 hamsters) and Δ*Ov-grn-1* flukes (3/13 hamsters).

There was no substantial difference in the location or subtype of CCA tumors among the treatment groups. The CCA tumors observed ranged in sizes from small neoplasms with multifocal distributions (10/24) to fully developed tumor masses visible to the unaided eye (14/24) (Figure 5). With respect to histological classification, 19 of 24 were of the tubular type (Brindley *et al.*, 2021). One papillary/cystic CCA was seen in the *ΔOv-grn-1* group and as was the mucinous type CCA in one SCR- and three *ΔOv-tsp-2 O. viverrini*-infected hamsters. The right lobe was the frequent location of the tumor in all hamsters (20/26), with nine in the left lobe, and three in the middle lobe. Occasionally, tumors had developed in more than one lobe (5/26) but usually occurred in a single lobe (21/26).

The pattern of pathogenesis in "moderate EPG" animals was similar to that for the SCR animals, showing dysplasia to CCA, with the most common pathogenesis of CCA in 78% of animals, and 100% of these were high grade (Figure 5H). No animals were excluded from the *ΔOv-grn-1* group and the 69% CCA rate was retained, of which 44% were high grade CCA. The *ΔOv-tsp-2* group changed substantially and resembled the SCR group when only "moderate EPG" animals were included. As with the SCR group hamsters, dysplasia was the minimum pathological lesion and 78% had CCA, with most (86%) being high grade CCA. We assessed pathology in relation to EPG levels (Figure 5I) and noted that low pathogenesis was observed in *ΔOv-tsp-2* hamsters with low EPG (<1,000). Beyond the arbitrary threshold of 1,000 EPG, |no correlation was apparent with level of pathology; the two SCR animals with the highest EPG recorded low grade CCA and degrees of dysplasia seen across the EPG range. Although we posit that at euthanasia 24 weeks after infection *ΔOv-tsp-2* group hamsters were infected with fewer adult stage liver flukes than the other groups, the similar pattern in hepatobiliary tract lesions in both the SCR and *ΔOv-tsp-2* groups with the moderate EPG phenotype indicated that the damage caused by chronic opisthorchiasis was similar, at and beyond a threshold number of parasites.

Subsequently, we focused assessments of histopathology only on the hamsters with the "moderate EPG" phenotype.

Reduced biliary tract fibrosis during infection with knockout parasites

Hepatic fibrosis was detected in Picro-Sirius Red (PSR)-stained thin tissue sections and enabled investigation and quantification of peribiliary fibrotic development (Figure 6A), using an automated, visual quantitation. Fibrosis was evaluated, firstly on Ishak stage, a semi-quantitative measure of the degree of fibrosis spread across the liver parenchyma (Goodman, 2007), and secondly, on the fibrotic deposition localized around the liver flukes, i.e., the amount of collagen deposition surrounding bile ducts occupied by parasites at the time of necropsy.

The Ishak scores correspond to degrees of damaging liver fibrosis and the levels reflect fibrotic expansion in periportal areas and the degree of bridging between portal regions, increasing up to level 6 with full cirrhosis (Figure 6B). The control (SCR) group was the most severely affected, with the livers of all hamsters assigned an Ishak score of 4. This indicated that fibrosis had progressed extensively with marked portal-portal and portal-central bridging. Hamsters in the *ΔOv-grn-1* group showed a median Ishak grade of 2 (range 2 to 4), with fibrosis in most portal areas with/without short fibrous septa that had not bridged to other portal regions. Hamsters infected with the *ΔOv-tsp-2* liver flukes showed a median Ishak score of 3 (range 2 to 4). This is defined as fibrous expansion of most portal areas with occasional bridging between them (Goodman, 2007). The *ΔOv-tsp-2* group was not significantly different to the control group, whereas the *ΔOv-grn-1* group had significantly less fibrosis compared to either SCR ($P \leq 0.0001$) or *ΔOv-tsp-2* ($P \leq 0.05$) groups.

To assess localized fibrosis specifically in the area where flukes were detected, we investigated the degree of periductal fibrosis immediately proximal to live flukes in the bile duct lumen. Automated analysis of the collagen deposition surrounding the bile ducts was undertaken using an ImageJ driven fibrosis quantification tool of the PSR-stained collagen. Of the bile duct tissue surrounding SCR and *ΔOv-tsp-2* flukes, 14.55% and 14.56% of the tissue was fibrotic, whereas 12.66% of bile duct tissue surrounding *ΔOv-grn-1* flukes was fibrotic (Figure 6C, $P \leq 0.05$).

***Ov-grn-1* gene edited flukes drive less cell proliferation than control flukes**

Here, we explored the *in vivo* effects as a consequence of programmed knockout of *Ov-grn-1* expression, following our earlier reports which centered on proliferation of the biliary epithelium and/or cultured cholangiocytes in response to *in vitro* exposure to *Ov*-GRN-1 (Bansal et al., 2017; Haugen et al., 2018; Papatpremsiri et al., 2015; Smout *et al.*, 2009; Smout et al., 2015). Proliferation of hamster biliary cells *in situ* was investigated using BrdU where the thymine analogue BrdU is incorporated into cellular DNA. Visualization was performed using immunohistochemistry (Figure 7A) and evaluated quantitatively. Concerning worm survival, and its corollary, the fitness cost of the programmed mutation, we examined proliferation but only in the bile ducts where flukes were situated. Median proliferation in bile duct tissue surrounding liver flukes in the SCR (15.0%) and *ΔOv-tsp-2* (11.1%) groups were not significantly different from each other, whereas only 3.1% of bile duct tissue surrounding *ΔOv-grn-1* flukes had incorporated BrdU ($P<0.0001$ vs SCR; $P<0.05$ vs *ΔOv-tsp-2*, Figure 7B). By contrast, the *ΔOv-grn-1* group (3.1%) showed significantly less proliferation than both the SCR, 4.8-fold reduction ($P<0.0001$) and the *ΔOv-tsp-2* group, 3.6-fold reduction ($P<0.05$).

Mutant *TP53* less frequent during infection with *Ov-grn-1* gene edited flukes

Tumor protein p53 plays a well-recognized role in cholangiocarcinogenesis and is highly expressed in fluke infection associated CCA cells (Brindley *et al.*, 2021; Jusakul et al., 2017). Brown nuclear staining pattern presents only in neoplastic biliary cells (Figure 7C). Wide angle images of flukes in the biliary tract showed mutant p53 positive and negative cells in the epithelium. The p53 staining was significantly different among the groups: SCR and *ΔOv-tsp-2* fluke infected hamsters showed 61.1 and 67.5% of cholangiocytes staining positive for p53 (not significant), respectively, whereas only 7.5% of cholangiocytes were positive in *ΔOv-grn-1* infected animals (~9-fold reduction, $P<0.01$) (Figure 7D).

Discussion

Cholangiocarcinoma (CCA) accounts for ~15% of all primary liver cancers and its incidence rates are increasing (Banales et al., 2020). Infection with the foodborne liver fluke, *Opisthorchis viverrini*, is the principal risk factor for CCA in the Lower Mekong River Basin countries including Thailand and Laos PDR (Brindley *et al.*, 2021; Petney et al., 2013; Sripa *et al.*, 2007). In an earlier report, we exploited this link to explore the role of a growth factor, liver fluke granulin, Ov-GRN-1, secreted by the parasite in tumorigenesis using programmed gene knockout, and reported that the infection was less severe although gene-edited parasites colonized the biliary tract of hamsters and developed into adult flukes (Arunsan *et al.*, 2019).

Here, we utilized an established model of opisthorchiasis-associated CCA in hamsters that were infected with the parasite during concurrent exposure to exogenous nitrosamine. CCA manifests under these conditions, and this rodent model reflects the human situation where chronic opisthorchiasis combined with a diet that is rich in fermented fish (in turn, rich in exogenous nitrosamines) culminates in high incidence of CCA (Mitacek et al., 1999; Sripa *et al.*, 2007; Sripa et al., 2015; Thamavit *et al.*, 1994). In hamsters, opisthorchiasis leads to periductal fibrosis. Severe periductal fibrosis combined with a nitric oxide carcinogen, such as DMN, results in epithelial cholangiocyte proliferation, hyperplasia, dysplasia, and DNA damage, eventually culminating in malignant transformation of the biliary tract (Lvova et al., 2012; Thamavit *et al.*, 1994). The current findings confirmed a role for *Ov*-GRN-1 in opisthorchiasis-associated malignancy. Markedly less proliferation of the biliary epithelium, mutant p53 expression in cholangiocytes, and periductal fibrosis were observed during infection with *ΔOv-grn-1* worms. Furthermore, we report a functional genomics approach-based expansion of the model pioneered more than 30 years ago (Thamavit *et al.*, 1987), which involved concurrent administration of nitrosamine during infection with gene-edited *O. viverrini*,

The fitness cost of gene knockout can be assessed from programmed gene editing, an approach that is employed for the unbiased identification of essential genes in other organisms and disease settings (Chai et al., 2020; Kim and Hart, 2021). Our present findings confirmed the power of RNA-guided targeted mutation to define essentiality and relevance of parasite proteins in

infection-associated morbidity and malignancy. The *Ov-grn-1* gene does not appear to essential for *in vivo* development and survival, which has enabled investigation here on the role of this protein in driving cell proliferation, pathology and ultimately contributing to CCA *in vivo*. Nonetheless, the reduced fecundity of *ΔOv-grn-1* liver flukes likely reflected a fitness deficit as the result of targeted gene knockout. By contrast, *Ov-tsp-2* appears to be essential to parasitism, since the *ΔOv-tsp-2* genotype did not survive, and sequencing of the indels across the relevant region of the genome confirmed that most of the surviving flukes from hamsters had undergone minimal or no editing of the *Ov-tsp-2* gene. These findings build upon earlier RNA interference-mediated silencing of *Ov-tsp-2* gene expression and the corresponding malformation of the tegument observed *in vitro* (Chaiyadet et al., 2017). Although *Ov-tsp-2* dsRNA-treated parasites were not used for *in vivo* studies, the damage to the tegument was extensive and survival *in vivo* of worms damaged to that extent appeared to be unlikely.

Although the primary goal of this investigation was to characterize pathogenesis and pathology associated with infection with *ΔOv-grn-1* flukes, and infection in the absence of Ov-GRN-1, we investigated the mutation profile induced by our gene-editing system. Intriguingly, most mutation in the *Ov-grn-1* targeted gene editing took place within the 5'UTR, and the majority (~99%) of the mutations centered on a single position (-9T) position, 28 bp 5' to the programmed CRISPR/Cas9 double strand break (DSB) at nucleotide positions 19 and 20 of the ORF. This was surprising, given that mutations were expected at the programmed DSB (Arunsan *et al.*, 2019). The *Ov-grn-1* 5'UTR does not correspond to regulatory sequences in the UTR database (http://utrdb.ba.itb.cnr.it/), which may not be unexpected given that few helminth parasite UTR regulatory elements have been characterized (International Helminth Genomes, 2019). Why this position was mutated is unclear; however, the marked reduction of transcription of *Ov-grn-1* that accompanied this mutation profile that, as noted, was focused within the 5'UTR, suggested that an active regulatory control element might be present.

Chronic liver fibrosis is a risk factor for liver cancer. The traditional lifestyle of people living in *O. viverrini*-endemic areas, notably a diet enriched in nitrosamines as well as routine use of alcohol, when coupled with the assault on the biliary epithelium by the attachment, feeding, movement, and secretions of the liver flukes that result in repeated cycles of injury and repair

cycles, establishes a compelling setting for malignant transformation (Fedorova et al., 2020; Sripa et al., 2012; Sripa et al., 2017). The secretion of liver fluke granulin into the bile ducts and its ability to relentlessly drive cell proliferation and to (re)heal wounds inflicted by the parasite plays a central role in this process (Smout *et al.*, 2015). Knockout mutation of *Ov-grn-1* did not substantially thwart infection, development and survival of the liver fluke *in vivo* but infection with these *ΔOv-grn-1* flukes failed to lead to the marked cell proliferation and fibrosis in the immediate vicinity of the parasites, and consequently fewer hamsters developed with high-grade CCA compared with the infections with the control SCR and *ΔOv-tsp-2* parasites. Indeed, more hamsters infected with *ΔOv-grn-1* flukes were diagnosed in the low-CCA and the proliferation categories than in the other treatment groups. Knockout mutation of *Ov-grn-1* attenuated virulence and impeded malignant transformation during chronic opisthorchiasis.

Infected hamsters exhibited elevated rates of *TP53* mutation although the level was markedly less during infection with *ΔOv-grn-1* flukes. The mutational signatures and related molecular pathways characteristic of human CCAs have been reviewed in depth, and the signature profiles differ between fluke associated and non-fluke associated CCAs (Brindley *et al.*, 2021). Fluke associated CCAs exhibit substantially more somatic mutations than non-fluke related CCAs (Jusakul *et al.*, 2017), likely the consequence of opisthorchiasis-associated chronic inflammation. In conformity with the human situation, reduced inflammation and fibrosis were seen in hamsters infected with the *ΔOv-grn-1* flukes, further emphasizing the virulence of this growth factor in chronic opisthorchiasis. Inactivating mutations of *TP53* are more prevalent in this subgroup, as are mutations of *ARID1A*, *ARID2*, *BRCA1* and *BRCA2*, than in non-fluke-related CCAs (Chaisaingmongkol et al., 2017; Chan-On et al., 2013; Jusakul *et al.*, 2017; Montal et al., 2020; Ong et al., 2012). In addition, hypermethylation has been noted for the promoter CpG islands of several other aberrantly expressed genes (Jusakul *et al.*, 2017).

Mosaicism of gene knock-out is a limitation of our somatic gene-editing approach. Obviating mosaicism by derivation of transgenic worms following germ line transgenesis is unlikely in the near future in the context of this multicellular eukaryote, especially when overlaid on the genetic complexity of a hermaphroditic platyhelminth parasite with a diploid genome. In addition, this parasite has a multiple host developmental cycle, which cannot reliably be reproduced in the

laboratory. Nonetheless, somatic genome editing is of increasing utility in biomedicine, including for treatment of hemoglobinopathies (Frangoul et al., 2021) and in the identification of targets for disease interventions (Fellmann et al., 2017). Given the role of *Ov*-GRN-1 as a virulence factor in opisthorchiasis, interventions that target this growth factor might be beneficial. Indeed, antibodies raised against recombinant *Ov*-GRN-1 block its ability to drive proliferation of CCA cell lines (Smout *et al.*, 2009), and vaccination strategies that target *Ov*-GRN-1 in the GI tract, for example through induction of mucosal IgA and IgG responses (Chaiyarit et al., 2011; Phumrattanaprapin et al., 2021) should be explored, and might form a valuable component of a multivalent, orally administered, anti-infection and anti-cancer vaccine (Brindley *et al.*, 2021; Phumrattanaprapin *et al.*, 2021).

STAR METHODS

Materials and methods

Metacercariae, newly excysted juvenile and adult developmental stages of *O .viverrini*

Metacercariae (MC) of *O .viverrini* were obtained from naturally infected cyprinid fish purchased from local food markets in the northeastern provinces of Thailand. MC were isolated from fishes by using pepsin digestion as described previously (Pinlaor et al., 2013). Briefly, whole fishes were minced by electric blender and digested with 0.25% pepsin with 1.5% HCl in 0.85% NaCl at 37 ºC for 120 min. The digested fishes were filtered sequentially through sieves of 1,100, 350, 250, and 140 µm mesh apertures. The filtered digest of fish flesh was subjected to gravity sedimentation in a sediment jar through several changes of 0.85% NaCl until the supernatant was clear. MC in the sediment were identified under a dissecting microscope as *O. viverrini* and active (larval movement within the cyst) *O. viverrini* MC were stored in 0.85% NaCl at 4ºC until used.

Newly excysted juveniles of *O. viverrini* (NEJ) were induced to escape from the metacercarial cyst by incubation in 0.25% trypsin in PBS supplemented with 2× 200 U/ml penicillin, 200

494 µg/ml streptomycin (2× Pen/Strep) for 5 min at 37°C in 5% CO_2 in air. NEJ were isolated free of
495 discarded cyst walls by mechanical passage through a 22 G needle (Arunsan *et al.*, 2019).
496
497 **Plasmid constructs and transfection of *O. viverrini* NEJ**
498
499 The CRISPR plasmid encoding a guide RNA (gRNA) complimentary to *Ov-grn-1* exon 1 termed
500 pCas-*Ov-grn-1* was constructed using the GeneArt CRISPR Nuclease Vector kit (Thermo Fisher
501 Scientific) as described (Arunsan *et al.*, 2019). The programmed cleavage site at nucleotide
502 position 1589–1608, 5'-GATTCATCTACAAGTGTTGA with a CGG proto-spacer adjacent
503 motif (PAM) which determined the cleavage site located at three nucleotides upstream on *Ov-*
504 *grn-1* was designed using the online tools, http://crispr.mit.edu/ (Ran et al., 2013) and
505 CHOPCHOP, http://chopchop.cbu.uib.no/ (Labun et al., 2016; Montague et al., 2014) using the
506 *Ov-grn-1* gene (6,287 bp, GenBank FJ436341.1) as the reference. A second plasmid, termed
507 pCas-*Ov-tsp-2* was constructed using the same approach; pCas-*Ov-tsp-2* encodes a gRNA
508 targeting exon 5 of the *Ov-tsp-2* gene (10,424 bp, GenBank JQ678707.1) (Laha et al., 2007;
509 Young et al., 2014). The guide RNAs encoded by *Ov-grn-1* and *Ov-tsp-2* exhibited high on-
510 target efficiency and little or no off-target matches to the *O. viverrini* genome. A third construct
511 termed pCas-*Ov*-scramble was also prepared and included as a control to normalize analysis of
512 gene expression and programmed gene knockout. The pCas-*Ov*-scramble construct included as
513 the gRNA, a transcript of 20 nt, 5'- GCACTACCAGAGCTAACTCA which exhibits only
514 minimal identity to the *O. viverrini* genome and which lack a PAM (Hulme et al., 2021). A
515 mammalian U6 promoter drives transcription of the gRNAs in all three plasmids and the CMV
516 promoter drives expression of the *Streptococcus pyogenes* Cas9 nuclease (modified to include
517 the eukaryotic nuclear localization signals 1 and 2). To confirm the orientation and sequences of
518 gRNA in the plasmid vector, *Escherichia coli* competent cells (TOP10) were transformed with
519 the plasmids, plasmid DNAs were recovered from ampicillin resistant colonies using a kit
520 (NucleoBond Xtra Midi, Macherey-Nagel GmbH, Düren, Germany), and the nucleotide
521 sequences of each construct confirmed as correct by Sanger direct cycle sequencing using a U6-
522 specific sequencing primer.
523

Two hundred NEJs of *O. viverrini* were dispensed into an electroporation cuvette, 4 mm gap (Bio-Rad, Hercules, CA) containing 20 µg pCas-*Ov-grn-1*, pCas-*Ov-tsp-2* or pCas-*Ov*-scramble in a total volume of 500 µl RPMI, and subjected to a single square wave pulse at 125 V for 20 ms (Gene Pulser Xcell, Bio-Rad). The NEJ were cultured in RPMI supplemented to 1% glucose for 60 min after which they were used for infection of hamsters by stomach gavage (below).

Infection of hamsters with gene edited NEJs

Figure 1 provides a timeline of the CCA model, employed in experiment 1 and 2. In a first experiment, nine male hamsters aged between 6-8 weeks were randomly divided into three experimental groups (Figure 1). Each hamster was infected with 100 *O. viverrini* NEJs. These NEJs had been transfected with pCas-*Ov-grn-1* plasmid, pCas-*Ov-tsp-2*, or the control pCas-*Ov*-scramble, and assigned the following identifiers: delta(Δ)-*gene* name, Δ*Ov-grn-1*, *ΔOv-tsp-2*, or SCR, respectively. These NEJs had been transfected with pCas-*Ov-grn-1* plasmid, pCas-*Ov-tsp-2*, or the control pCas-*Ov*-scramble, and assigned the following identifiers: delta(Δ)-*gene* name, Δ*Ov-grn-1*, *ΔOv-tsp-2*, or SCR, respectively. The hamsters were infected with NEJ by gastric gavage The infected hamsters were maintained under a standard light cycle (12 hours dark/light) with access to water and food *ad libitum*. At day 14 following infection, the water accessed by the hamsters was replaced with drinking water supplemented with dimethylnitrosamine (DMN) (synonym, *N*-nitrosodimethylamine) (Sigma-Aldrich, Inc., St. Louis, MO) at 12.5 ppm, which was maintained until 10 weeks following infection (Loilome *et al.*, 2006; Thamavit *et al.*, 1987; Thamavit *et al.*, 1994). Hamster feces were collected at weeks 10 and 12 after infection for fecal egg counts. The hamsters were euthanized at week 14 after infection via isoflurane inhalation, livers were collected, and numbers of liver flukes counted.

In the second experiment, 45 male Syrian golden hamsters, *Mesocricetus auratus*, 6–8 weeks of age, were randomly divided into three groups each with 15 hamsters and infected with gene edited NEJs (above). These NEJs had been transfected with pCas-*Ov-grn-1* plasmid, pCas-*Ov-tsp-2*, or the control pCas-*Ov*-scramble, and assigned the following identifiers: delta(Δ)-*gene* name, Δ*Ov-grn-1*, *ΔOv-tsp-2*, or SCR, respectively. The NEJ were introduced into the hamster stomach using an orogastric tube. The infected hamsters were maintained under a standard light

cycle (12 hours dark/light) with access to water and food *ad libitum*. At day 14 following infection, the water accessed by the hamsters was replaced with drinking water supplemented with DMN at 12.5 ppm, which was maintained until 10 weeks following infection, as above. Hamster feces were collected at week 23 after infection for fecal egg counts. At week 24, 40 mg/kg thymine analogue 5-bromo-2'-deoxyuridine (BrdU, Abcam, College Science Park, UK) was introduced into the peritoneum of the hamsters at 30 min before euthanasia,, to incorporate the thymidine analogue into the nuclei to enable investigation of proliferation of the biliary epithelia post-mortem (Suyapoh et al., 2021). Hamsters were euthanized, the liver resected from each hamster at necropsy, the liver lobes separated, and the left, middle and right lobes fixed in 10% formalin. We have used the shorthand to identify the lobes; left (left dorsocaudal), middle (combined ventral and dorsal median lobes), and right (right dorsocaudal). Liver flukes recovered from the hepatobiliary tract were stored in RNAlater (Thermo Fisher) for subsequent analysis of gene expression, gene-editing efficiency, and indel profile.

All the hamsters were maintained at the animal rearing facility of the Faculty of Medicine, Khon Kaen University, Khon Kaen. The protocol was approved by the Animal Ethics Committee of Khon Kaen University, approval number ACUC-KKU-61/60, which adhered to the guidelines prescribed by the National Research Council of Thailand for the Ethics of Animal Experimentation.

Histopathological investigation of hepatobiliary tissues

Whole hamster livers were dissected and fixed in 10% buffered formalin. After overnight fixation, specimens were further routinely processed for paraffin embedding by dehydration in a series of 70%, 90%, and 100% ethanol, cleared in xylene and infiltrated in melted paraffin before being embedded in paraffin block. Four μm liver sections were obtained using a microtome and stained with hematoxylin and eosin (H&E) for histopathologic evaluation of the hepatobiliary system. Histopathological grading criteria of the liver and bile duct of hamsters was scored for the extent of bile duct inflammation, bile duct changes, dysplasia (including dysplasia in cholangiofibrosis) and stage of CCA as described (Lvova *et al.*, 2012; Sato et al., 2014; Sudsarn et al., 2016; Zen et al., 2007), with modifications (Table 1).

Table 1. Criteria for histopathological and histochemical assessment

Histopathological lesion	Grade description	Reference
Inflammation	0 = None (no/minimal liver tissue or portal inflammation) 1 = Mild (1-2 foci per 4× objective at hepatocyte & periportal area) 2 = Moderate (3-5 foci per 4× objective at hepatocyte & periportal area) 3 = Severe (> 5 foci per 4× objective at hepatocyte & periportal area)	(Lvova *et al.*, 2012; Sudsarn *et al.*, 2016; Sudsarn et al., 2014)
Bile duct changes	0 = None (absent proliferation and cholangiofibrosis) 1 = Mild (bile duct proliferation without cholangiofibrosis or periductal fibrosis) 2 = Moderate (bile duct proliferation with cholangiofibrosis) 3 = Severe (bile duct proliferation with cholangiofibrosis and periductal fibrosis)	(Lvova *et al.*, 2012; Sudsarn *et al.*, 2016; Sudsarn *et al.*, 2014)
Dysplasia	0 = None (No cellular atypia, no nuclear polarity, no protruding of nuclei, no nuclear pseudostratification) 1 = Mild (Cellular atypia+, no nuclear polarity, no protruding of nuclei, nuclear pseudostratification+, nuclei within the lower two-thirds) 2 = Moderate (Cellular atypia+, nuclear polarity+, protruding of nuclei+, nuclear pseudostratification+) 3 = High (Cellular atypia++, nuclear polarity++, protruding of nuclei+, nuclear pseudostratification+)	(Sato *et al.*, 2014)
Cholangiocarcinoma	0 = None (no evident of CCA) Low CCA: 1 = Mild (CCA area 1-2 foci per 4× objective) High CCA: combined 2+3: 2 = Moderate (CCA area 3-5 foci per 4× objective) and 3 = Severe (CCA area> 5 foci per 4× objective)	(Lvova *et al.*, 2012; Sudsarn *et al.*, 2016; Sudsarn *et al.*, 2014)
Fibrosis (PSR stain):	0 =No fibrosis	(Ishak et al., 1995)

Ishak score	1 = Fibrous expansion of some portal areas, with or without short fibrous septa 2 = Fibrous expansion of most portal areas, with or without short fibrous septa 3 = Fibrous expansion of most portal areas with occasional portal to portal bridging 4 = Fibrous expansion of portal areas with marked bridging (portal to portal as well as portal to central) 5 = Marked bridging (portal–portal and/or portal–central) with occasional nodules (incomplete cirrhosis) 6 = Cirrhosis, probable or definite	(Goodman, 2007)
Assessment of collagen proximal to liver flukes	Quantitative automated evaluation of collagen deposition percentage surrounding bile ducts	ImageJ software "MRI Fibrosis quantification tool" macro (Volker Bäcker 2015, (INSERM; Montpellier RIO Imaging, www.mri.cnrs.fr

Fecal egg counts and worm counts

Feces from each hamster was individually collected, weighed and *O. viverrini* eggs per gram of feces (EPG) calculated using a modified formalin-ethyl acetate technique (Elkins et al., 1986). In brief, hamster feces were collected and fixed in 10 ml of 10% formalin. Thereafter, the slurry of formalin-fixed feces was filtered through two layers of gauze, and clarified by centrifugation at 500 *g* for 2 min. The pellet was resuspended with 7 ml of 10% formalin, mixed with 3 ml ethyl-acetate and pelleted at 500 *g* for 5 min. The pellet was resuspended in 10% formalin solution and examined at 400× by light microscopy. EPG was calculated as follows: (average number eggs × total drops of fecal solution)/ gram of feces. To recover the adult liver flukes, food was withdrawn from the hamsters 16 hours before euthanasia. At necropsy, terminal blood was collected from the heart and allowed to clot at 4˚C for 30 min followed by centrifugation at 2,100

g for 10 min. The clotted-blood serum was stored at -20˚C. Intact mature *O. viverrini* from the hepatobiliary tract were recovered during observation of the livers using a stereo dissecting microscope and stored for downstream gene-editing investigation.

Extraction of nucleic acids

Pooled NEJ or single mature worms from either experimental or control groups were homogenized in RNAzol RT (Molecular Research Center, Inc., Cincinnati, OH) before dual RNA and DNA extraction as described (Arunsan *et al.*, 2019). Briefly, the parasite(s) were homogenized in RNAzol RT using a motorized pestle, after which the DNA and protein were precipitated in nuclease free water. The aqueous upper phase was transferred into a new tube for total RNA precipitation by isopropanol (50% v/v). The DNA/protein pellet was resuspended in DNAzol and genomic DNA extracted according to the manufacturer's instructions (Molecular Research Center). Concentration and integrity of genomic DNA and total RNA were independently quantified by spectrophotometry (NanoDrop 1000, Thermo Fisher, Waltham, MA). Transcription and expression were investigated in pools of NEJs and in individual adult flukes after normalization with the controls.

Quantitative real-time PCR

cDNA was synthesized from DNase I-treated-total RNA (10 ng) using Maxima First Strand cDNA synthesis with a DNase kit (Thermo Scientific) prior to performing quantitative real-time PCR (qPCR). Each cDNA sample was prepared for qPCR in triplicate using SSoAdvanced Universal SYBR Green Supermix (Bio-Rad). Each qPCR reaction consisted of 5 µl of SYBR Green Supermix, 0.2 µl (10 µM) each of specific forward and reverse primers for *Ov-grn-1* (forward primer, *Ov*-GRN-1-RT-F: 5'-GACTTGTTGTCGCGGCTTAC-3' and reverse primer, *Ov*-GRN1-RT-R: 5'-CGCGAAAGTAGCTTGTGGTC-3'), amplifying 147 base pairs (bp) of 444 nt of *Ov-grn-1* mRNA, complete cds GenBank FJ436341.1) or primers for *Ov-tsp-2* (forward primer, *Ov-TSP-2*-F 5'- ACAAGTCGTATGTGGAATCA- 3' and reverse primer *Ov-TSP-2*-R 5'- CCGTCTCGCCTTCTCCTTT- 3', product size 377 bp of 672 nt of *Ov-tsp-2*A mRNA, complete cds (GenBank JQ678707.1), 2 µl of cDNA and distilled water to a final volume of 10 µl were used in the reaction. The thermal cycle was a single initiation cycle at

632 95°C for 10 min followed by 40 cycles of denaturation at 95°C for 15s, annealing at 55°C for 30s
633 using CFX Connect Real-Time PCR system (Bio-Rad). The endogenous actin gene (1301 nt of
634 *Ov-actin* mRNA, GenBank EL620339.1) was used as a reference (Papatpremsiri *et al.*, 2015;
635 Piratae et al., 2012; Schmittgen and Livak, 2008) (forward primer, *Ov*-actin-F: 5'-
636 AGCCAACCGAGAGAAGATGA and reverse primer, *Ov*-actin-R: 5'-
637 ACCTGACCATCAGGCAGTTC. The fold change in *Ov-grn-1* and *Ov-tsp*-2 transcripts was
638 calculated using the $2^{(-\Delta\Delta Ct)}$ method using the *Ov-actin* gene as a reference for normalization
639 (Papatpremsiri *et al.*, 2015; Piratae *et al.*, 2012; Schmittgen and Livak, 2008).
640
641 **Illumina based targeted next generation sequencing of targeted amplicons**
642
643 The Amplicon-EZ next generation sequencing service (GENEWIZ, South Plainfield, NJ) was
644 used to obtain deeper coverage of the exon 1 from individual mature worms or pooled NEJ,
645 providing >50,000 reads per sample. A 173 nucleotide region flanking the programmed DSB
646 was amplified with forward primer 5'-TTCGAGATTCGGTCAGCCG-3' and reverse primer 5'-
647 GCACCAACTCGCAACTTACA-3', and was sequenced directly using Illumina chemistry. The
648 CRISPR-sub web platform (http://www.rgenome.net/crispr-sub/#!) analysis with comparison
649 range 60 nt was used to screen for Cas9-mediated substitutions in the reads, with comparisons
650 among the treatment groups (Hwang et al., 2020b). In addition, CRISPResso2 with 30 nt
651 quantification window (Clement *et al.*, 2019) was employed for indel estimation, as described
652 (Arunsan *et al.*, 2019). The NGS reads are available at GenBank Bioproject PRJNA385864,
653 BioSample SAMN07287348, SRA study PRJNA385864, accessions SRR 15906234-15906251.
654
655 **BrdU-staining for proliferation of biliary epithelial cells**
656
657 Proliferation of biliary epithelial cells was investigated by using incorporation of BrdU. In brief,
658 the liver sections of a paraffin-embedded sample were soaked in xylene, rehydrated in graded
659 alcohol solution (100%, 90%, and 70% ethanol for 5 min each), and antigen was retrieved in
660 citrate buffer (pH 6) for 5 min in a high-pressure cooker. The tissue sections were blocked with
661 3% H_2O_2 in methanol for 30 min and subsequently incubated with 5% fetal bovine serum in
662 phosphate buffered saline for 30 min at room temperature (RT). The sections were incubated

with monoclonal mouse anti-BrdU (Abcam, catalogue no. ab8955) diluted 1:200 in PBS at 4°C overnight, and then probed with goat anti-mouse IgG-HRP (Invitrogen, Thermo Fisher) diluted 1:1,000 in PBS for 60 min at RT. The peroxidase reaction was developed with 3, 3'-diaminobenzidine (DAB). Sections were counterstained with Mayer's hematoxylin for 5 min before dehydrating and mounting. A positive signal was indicated by a brown color under light microscopy. The image was captured by a Zeiss Axiocam microscope camera ICc5 and NIS-Element software (Nikon, Japan). To quantify BrdU-positive nuclei, cholangiocytes were counted in 10 non-overlapping fields of 400x magnification, with a total of 1,000 biliary cholangiocytes counted using the counter plug-in of ImageJ 1.52P. The cell proliferation index was calculated as a percentage using the formula: positive biliary nuclei/total biliary cells x100%.

Immunohistochemical staining for mutant forms of p53

To investigate levels of p53 mutation (Surget et al., 2013) in cholangiocytes, paraffin-embedded tissue sections were deparaffinized and rehydrated by standard methods. Thereafter, sections were incubated with monoclonal mouse anti-p53 (mutant, clone Ab-3 PAb240 catalogue no. OP29-200UG) (Merck, Darmstadt, Germany) diluted 1:100 in PBS at 4°C overnight , and after thorough washing, probed with goat anti-mouse IgG-HRP (Invitrogen, Carlsbad, CA) diluted 1:1,000 in PBS for 60 min at 25°C. The peroxidase reaction was developed with 3,3'- DAB and sections counterstained with Mayer's hematoxylin for 5 min. A human CCA cell line served as the positive control for p53 positivity (Batheja et al., 2000; Nakayama and Oshima, 2018). Images of high-power fields (400x magnification) of the biliary epithelium were taken in five non-overlapping fields of each of the right, middle, and left liver lobes using a Zeiss Axiocam fitted with a ICc5 camera and NIS-Element software (Nikon). The percentage of mutant p53-positive cholangiocytes was determined by calculating positive cells from 500 to 800 cholangiocytes from the right, middle, and left lobes of the liver using imageJ.

PSR staining for fibrosis evaluation

Liver tissue sections where *O. viverrini* reside were selected for fibrosis measurements with PSR (Abcam, catalogue ab150681). The thin sections were deparaffinized in xylene and rehydrated through an ethanol gradient. PSR solution was applied to the sections and incubated at 25°C for 60 min. Excess dye was removed by washing twice in dilute acetic acid (0.5%) after which sections were dehydrated through graded series of ethanol and xylene, the slides cleared with 100% xylene, mounted in Per-mount, and air dried overnight. Fibrosis around the bile duct (periductal fibrosis, PF) proximal to the liver flukes was evaluated by two approaches: first, by scoring according to accepted criteria (Goodman, 2007; Ishak *et al.*, 1995). Samples were blinded and fibrosis scores (0-6) were graded semi-quantitatively by Ishak stage (Table 1) by two experienced pathologists. Second, localized fibrosis was evaluated by capturing images for quantification of collagen deposition. Specifically, the PSR-stained fibrotic lesions was measured using the plug-in fibrosis tool developed by Volker Bäcker (New FUJI toolsets for bioimage analysis, DOI:10.13140/RG.2.2.15064.60167, available at https://github.com/MontpellierRessourcesImagerie/imagej_macros_and_scripts/wiki/MRI_Fibrosis_Tool. We (Arunsan *et al.*, 2019) and others (Hollenbach et al., 2017; Rabacal et al., 2019) have used this tool with PSR-stained tissues.

Statistical analysis

One-way ANOVA with Tukey multiple comparisons was used for comparisons with 2-4 replicates (NEJ transcripts, worm burden, 14 week EPG). The Krustal-Wallis non parametric test with Dunn's multiple comparisons was used for datasets that were not normally distributed including transcripts in adult liver flukes at weeks 14 and 24, 24-week EPGs, Ishak and periductal fibrosis, BrdU, and anti-mutant p53 signals. Replicates are shown with the mean and standard error of the mean (x±SEM) bars or as median with interquartile ranges for non-normal distributions. Statistical analysis and graphic presentation of the results were undertaken using GraphPad Prism version 9 (GraphPad Software Inc, San Diego, CA). As indel % values did not have replicates for the SCR group, a one sample *t* test for either NEJs or adult *O. viverrini* worms comparing values for the *ΔOv-grn-1* and the corresponding SCR group was used. The correlation between % indel and transcript levels was assessed using a two-tailed non-parametric Spearman correlation co-efficient (r_s). Values of $P \leq 0.05$ were considered to be statistically

significant; the asterisks (*) correspond to the SCR vs *ΔOv-grn-1* group comparisons; *, *P*0.05, **, *P* ≤0.01, ***, *P* ≤0.001, ****, *P* ≤0.0001; hashes (#) to *ΔOv-grn-1* vs *ΔOv-tsp-2* group comparisons; #, *P* ≤0.05; ##, *P* ≤0.01; ###, *P*≤0.00; ####, *P* ≤0.0001.

Acknowledgements

We thank Suwit Balthaisong for technical assistance. This study was supported by the Research Program, Research and Graduate Studies, Khon Kaen University to SC, ST and TL), the National Cancer Institute, National Institutes of Health (NIH) USA award R01CA164719 (AL, TL, PJB,) and the Australian National Health and Medical Research Council (NHMRC award APP1085309 to AL, JS and TL, and senior principal research fellowship APP1117504 to AL). This research was funded in part, by the Wellcome Trust (WT), grant number 107475/Z/15/Z. For the purpose of Open Access, the authors have applied a CC BY public copyright license to any Author Accepted Manuscript version arising from this submission. The content is solely the responsibility of the authors and does not necessarily represent the official views of the NCI, NIH, NHMRC, or WT.

Author contributions

T. Laha, A. Loukas, P. Brindley, S. Tangkawattana, S. Chaiyadet, W. Ittiprasert, P. Arunsan, and M. Smout conceived and designed the research; S. Chaiyadet, S. Tangkawattana, R. Deenonpoe, V. Mann, M. Smout, and W. Ittiprasert performed the research; S. Chaiyadet, S. Tangkawattana, R. Deenonpoe, and M. Smout recorded the findings ; T. Laha, P.J. Brindley, A. Loukas, M. Smout and W. Ittiprasert contributed reagents and analytical tools; T. Laha, S. Chaiyadet, P. Arunsan, S. Tangkawattana, V. Mann, M. Smout, and W. Ittiprasert completed the experiments; S. Chaiyadet, S. Tangkawattana, W. Ittiprasert, and M. Smout analyzed data; S. Chaiyadet, S. Tangkawattana, T. Laha, P. Brindley, W. Ittiprasert, M. Smout, and A. Loukas prepared figures and wrote the paper.

Author ORCiD

Wannaporn Ittiprasert, http://orcid.org/0000-0001-9411-8883

Michael J. Smout, https://orcid.org/0000-0001-6937-0112
Paul J. Brindley, https://orcid.org/0000-0003-1765-0002
Alex Loukas, https://orcid.org/0000-0002-0896-8441

stintere Conflict of. The authors declare that this study was performed without any commercial or financial relationships construable as potential conflicts of interest.

References

Arunsan, P., Ittiprasert, W., Smout, M.J., Cochran, C.J., Mann, V.H., Chaiyadet, S., Karinshak, S.E., Sripa, B., Young, N.D., Sotillo, J., et al. (2019). Programmed knockout mutation of liver fluke granulin attenuates virulence of infection-induced hepatobiliary morbidity. Elife *8*. 10.7554/eLife.41463.

Banales, J.M., Marin, J.J.G., Lamarca, A., Rodrigues, P.M., Khan, S.A., Roberts, L.R., Cardinale, V., Carpino, G., Andersen, J.B., Braconi, C., et al. (2020). Cholangiocarcinoma 2020: the next horizon in mechanisms and management. Nature Reviews Gastroenterology & Hepatology *17*, 557-588. 10.1038/s41575-020-0310-z.

Bansal, P.S., Smout, M.J., Wilson, D., Cobos Caceres, C., Dastpeyman, M., Sotillo, J., Seifert, J., Brindley, P.J., Loukas, A., and Daly, N.L. (2017). Development of a Potent Wound Healing Agent Based on the Liver Fluke Granulin Structural Fold. J Med Chem *60*, 4258-4266. 10.1021/acs.jmedchem.7b00047.

Batheja, N., Suriawinata, A., Saxena, R., Ionescu, G., Schwartz, M., and Thung, S.N. (2000). Expression of p53 and PCNA in Cholangiocarcinoma and Primary Sclerosing Cholangitis. Modern Pathology *13*, 1265-1268. 10.1038/modpathol.3880231.

Brindley, P.J., Bachini, M., Ilyas, S.I., Khan, S.A., Loukas, A., Sirica, A.E., Teh, B.T., Wongkham, S., and Gores, G.J. (2021). Cholangiocarcinoma. Nat Rev Dis Primers *7*, 65. 10.1038/s41572-021-00300-2.

Brindley, P.J., da Costa, J.M., and Sripa, B. (2015). Why does infection with some helminths cause cancer? Trends Cancer *1*, 174-182. 10.1016/j.trecan.2015.08.011.

Chai, A.W.Y., Yee, P.S., Price, S., Yee, S.M., Lee, H.M., Tiong, V.K., Goncalves, E., Behan, F.M., Bateson, J., Gilbert, J., et al. (2020). Genome-wide CRISPR screens of oral squamous cell carcinoma reveal fitness genes in the Hippo pathway. Elife *9*. 10.7554/eLife.57761.

Chaisaingmongkol, J., Budhu, A., Dang, H., Rabibhadana, S., Pupacdi, B., Kwon, S.M., Forgues, M., Pomyen, Y., Bhudhisawasdi, V., Lertprasertsuke, N., et al. (2017). Common Molecular Subtypes Among Asian Hepatocellular Carcinoma and Cholangiocarcinoma. Cancer Cell *32*, 57-70 e53. 10.1016/j.ccell.2017.05.009.

Chaiyadet, S., Krueajampa, W., Hipkaeo, W., Plosan, Y., Piratae, S., Sotillo, J., Smout, M., Sripa, B., Brindley, P.J., Loukas, A., and Laha, T. (2017). Suppression of mRNAs encoding CD63 family tetraspanins from the carcinogenic liver fluke Opisthorchis viverrini results in distinct tegument phenotypes. Sci Rep *7*, 14342. 10.1038/s41598-017-13527-5.

Chaiyadet, S., Smout, M., Johnson, M., Whitchurch, C., Turnbull, L., Kaewkes, S., Sotillo, J., Loukas, A., and Sripa, B. (2015). Excretory/secretory products of the carcinogenic liver fluke are endocytosed by human cholangiocytes and drive cell proliferation and IL6 production. Int J Parasitol *45*, 773-781. 10.1016/j.ijpara.2015.06.001.

Chaiyarit, P., Sithithaworn, P., Thuwajit, C., and Yongvanit, P. (2011). Detection of salivary antibodies to crude antigens of Opisthorchis viverrini in opisthorchiasis and cholangiocarcinoma patients. Clin Oral Investig *15*, 477-483. 10.1007/s00784-010-0421-y.

Chan-On, W., Nairismagi, M.L., Ong, C.K., Lim, W.K., Dima, S., Pairojkul, C., Lim, K.H., McPherson, J.R., Cutcutache, I., Heng, H.L., et al. (2013). Exome sequencing identifies distinct mutational patterns in liver fluke-related and non-infection-related bile duct cancers. Nat Genet *45*, 1474-1478. 10.1038/ng.2806.

Clement, K., Rees, H., Canver, M.C., Gehrke, J.M., Farouni, R., Hsu, J.Y., Cole, M.A., Liu, D.R., Joung, J.K., Bauer, D.E., and Pinello, L. (2019). CRISPResso2 provides accurate and rapid genome editing sequence analysis. Nat Biotechnol *37*, 224-226. 10.1038/s41587-019-0032-3.

Elkins, D.B., Haswell-Elkins, M., and Anderson, R.M. (1986). The epidemiology and control of intestinal helminths in the Pulicat Lake region of Southern India. I. Study design and pre- and post-treatment observations on Ascaris lumbricoides infection. Trans R Soc Trop Med Hyg *80*, 774-792. 10.1016/0035-9203(86)90384-6.

Elkins, D.B., Sithithaworn, P., Haswell-Elkins, M., Kaewkes, S., Awacharagan, P., and Wongratanacheewin, S. (1991). Opisthorchis viverrini: relationships between egg counts, worms recovered and antibody levels within an endemic community in northeast Thailand. Parasitology *102 Pt 2*, 283-288. 10.1017/s0031182000062600.

Fedorova, O.S., Fedotova, M.M., Zvonareva, O.I., Mazeina, S.V., Kovshirina, Y.V., Sokolova, T.S., Golovach, E.A., Kovshirina, A.E., Konovalova, U.V., Kolomeets, I.L., et al. (2020). Opisthorchis felineus infection, risks, and morbidity in rural Western Siberia, Russian Federation. PLoS Negl Trop Dis *14*, e0008421. 10.1371/journal.pntd.0008421.

Fellmann, C., Gowen, B.G., Lin, P.C., Doudna, J.A., and Corn, J.E. (2017). Cornerstones of CRISPR-Cas in drug discovery and therapy. Nat Rev Drug Discov *16*, 89-100. 10.1038/nrd.2016.238.

Frangoul, H., Altshuler, D., Cappellini, M.D., Chen, Y.S., Domm, J., Eustace, B.K., Foell, J., de la Fuente, J., Grupp, S., Handgretinger, R., et al. (2021). CRISPR-Cas9 Gene Editing for Sickle Cell Disease and β-Thalassemia. N Engl J Med *384*, 252-260. 10.1056/NEJMoa2031054.

Goodman, Z.D. (2007). Grading and staging systems for inflammation and fibrosis in chronic liver diseases. J Hepatol *47*, 598-607. 10.1016/j.jhep.2007.07.006.

Haugen, B., Karinshak, S.E., Mann, V.H., Popratiloff, A., Loukas, A., Brindley, P.J., and Smout, M.J. (2018). Granulin Secreted by the Food-Borne Liver Fluke Opisthorchis viverrini Promotes Angiogenesis in Human Endothelial Cells. Front Med (Lausanne) *5*, 30. 10.3389/fmed.2018.00030.

Hollenbach, M., Thonig, A., Pohl, S., Ripoll, C., Michel, M., and Zipprich, A. (2017). Expression of glyoxalase-I is reduced in cirrhotic livers: A possible mechanism in the development of cirrhosis. PLoS One *12*, e0171260. 10.1371/journal.pone.0171260.

Hulme, B.J., Geyer, K.K., Forde-Thomas, J.E., Padalino, G., Phillips, D.W., Ittiprasert, W., Karinshak, S.E., Mann, V.H., Chalmers, I.W., Brindley, P.J., et al. (2021). Schistosoma mansoni α-N-acetylgalactosaminidase (SmNAGAL) regulates coordinated parasite movement and egg production. bioRxiv, 2021.2007.2026.453800. 10.1101/2021.07.26.453800.

Hwang, G.-H., Yu, J., Yang, S., Son, W.J., Lim, K., Kim, H.S., Kim, J.-S., and Bae, S. (2020a). CRISPR-sub: Analysis of DNA substitution mutations caused by CRISPR-Cas9 in human cells. Computational and Structural Biotechnology Journal *18*, 1686-1694. https://doi.org/10.1016/j.csbj.2020.06.026.

Hwang, G.H., Yu, J., Yang, S., Son, W.J., Lim, K., Kim, H.S., Kim, J.S., and Bae, S. (2020b). CRISPR-sub: Analysis of DNA substitution mutations caused by CRISPR-Cas9 in human cells. Comput Struct Biotechnol J *18*, 1686-1694. 10.1016/j.csbj.2020.06.026.

IARC (2012). Biological agents. Volume 100 B. A review of human carcinogens. IARC monographs on the evaluation of carcinogenic risks to humans *100*, 1-441.

International Helminth Genomes, C. (2019). Comparative genomics of the major parasitic worms. Nat Genet *51*, 163-174. 10.1038/s41588-018-0262-1.

Ishak, K., Baptista, A., Bianchi, L., Callea, F., De Groote, J., Gudat, F., Denk, H., Desmet, V., Korb, G., MacSween, R.N., and et al. (1995). Histological grading and staging of chronic hepatitis. J Hepatol *22*, 696-699. 10.1016/0168-8278(95)80226-6.

Jusakul, A., Cutcutache, I., Yong, C.H., Lim, J.Q., Huang, M.N., Padmanabhan, N., Nellore, V., Kongpetch, S., Ng, A.W.T., Ng, L.M., et al. (2017). Whole-Genome and Epigenomic Landscapes of Etiologically Distinct Subtypes of Cholangiocarcinoma. Cancer Discov *7*, 1116-1135. 10.1158/2159-8290.CD-17-0368.

Kim, E., and Hart, T. (2021). Improved analysis of CRISPR fitness screens and reduced off-target effects with the BAGEL2 gene essentiality classifier. Genome Med *13*, 2. 10.1186/s13073-020-00809-3.

Kim, J.H., Choi, M.H., Bae, Y.M., Oh, J.K., Lim, M.K., and Hong, S.T. (2011). Correlation between discharged worms and fecal egg counts in human clonorchiasis. PLoS Negl Trop Dis *5*, e1339. 10.1371/journal.pntd.0001339.

Kitadokoro, K., Bordo, D., Galli, G., Petracca, R., Falugi, F., Abrignani, S., Grandi, G., and Bolognesi, M. (2001). CD81 extracellular domain 3D structure: insight into the tetraspanin superfamily structural motifs. EMBO J *20*, 12-18. 10.1093/emboj/20.1.12.

Labun, K., Montague, T.G., Gagnon, J.A., Thyme, S.B., and Valen, E. (2016). CHOPCHOP v2: a web tool for the next generation of CRISPR genome engineering. Nucleic Acids Research *44*, W272-W276. 10.1093/nar/gkw398.

Laha, T., Pinlaor, P., Mulvenna, J., Sripa, B., Sripa, M., Smout, M.J., Gasser, R.B., Brindley, P.J., and Loukas, A. (2007). Gene discovery for the carcinogenic human liver fluke, Opisthorchis viverrini. BMC Genomics *8*, 189. 10.1186/1471-2164-8-189.

Loilome, W., Yongvanit, P., Wongkham, C., Tepsiri, N., Sripa, B., Sithithaworn, P., Hanai, S., and Miwa, M. (2006). Altered gene expression in Opisthorchis viverrini-associated cholangiocarcinoma in hamster model. Molecular carcinogenesis *45*, 279-287. 10.1002/mc.20094.

Lvova, M.N., Tangkawattana, S., Balthaisong, S., Katokhin, A.V., Mordvinov, V.A., and Sripa, B. (2012). Comparative histopathology of Opisthorchis felineus and Opisthorchis viverrini in a hamster model: an implication of high pathogenicity of the European liver fluke. Parasitol Int *61*, 167-172. 10.1016/j.parint.2011.08.005.

Mitacek, E.J., Brunnemann, K.D., Suttajit, M., Martin, N., Limsila, T., Ohshima, H., and Caplan, L.S. (1999). Exposure to N-nitroso compounds in a population of high liver cancer regions in Thailand: volatile nitrosamine (VNA) levels in Thai food. Food Chem Toxicol *37*, 297-305. 10.1016/s0278-6915(99)00017-4.

Montague, T.G., Cruz, J.M., Gagnon, J.A., Church, G.M., and Valen, E. (2014). CHOPCHOP: a CRISPR/Cas9 and TALEN web tool for genome editing. Nucleic Acids Research *42*, W401-W407. 10.1093/nar/gku410.

Montal, R., Sia, D., Montironi, C., Leow, W.Q., Esteban-Fabro, R., Pinyol, R., Torres-Martin, M., Bassaganyas, L., Moeini, A., Peix, J., et al. (2020). Molecular classification and therapeutic targets in extrahepatic cholangiocarcinoma. J Hepatol *73*, 315-327. 10.1016/j.jhep.2020.03.008.

Nakayama, M., and Oshima, M. (2018). Mutant p53 in colon cancer. Journal of Molecular Cell Biology *11*, 267-276. 10.1093/jmcb/mjy075.

Ong, C.K., Subimerb, C., Pairojkul, C., Wongkham, S., Cutcutache, I., Yu, W., McPherson, J.R., Allen, G.E., Ng, C.C., Wong, B.H., et al. (2012). Exome sequencing of liver fluke-associated cholangiocarcinoma. Nat Genet *44*, 690-693. 10.1038/ng.2273.

Papatpremsiri, A., Smout, M.J., Loukas, A., Brindley, P.J., Sripa, B., and Laha, T. (2015). Suppression of Ov-grn-1 encoding granulin of Opisthorchis viverrini inhibits proliferation of biliary epithelial cells. Exp Parasitol *148*, 17-23. 10.1016/j.exppara.2014.11.004.

Petney, T.N., Andrews, R.H., Saijuntha, W., Wenz-Mucke, A., and Sithithaworn, P. (2013). The zoonotic, fish-borne liver flukes Clonorchis sinensis, Opisthorchis felineus and Opisthorchis viverrini. Int J Parasitol *43*, 1031-1046. 10.1016/j.ijpara.2013.07.007.

Phumrattanaprapin, W., Chaiyadet, S., Brindley, P.J., Pearson, M., Smout, M.J., Loukas, A., and Laha, T. (2021). Orally Administered Bacillus Spores Expressing an Extracellular Vesicle-Derived Tetraspanin Protect Hamsters Against Challenge Infection With Carcinogenic Human Liver Fluke. J Infect Dis *223*, 1445-1455. 10.1093/infdis/jiaa516.

Pinlaor, S., Onsurathum, S., Boonmars, T., Pinlaor, P., Hongsrichan, N., Chaidee, A., Haonon, O., Limviroj, W., Tesana, S., Kaewkes, S., and Sithithaworn, P. (2013). Distribution and abundance of Opisthorchis viverrini metacercariae in cyprinid fish in Northeastern Thailand. The Korean journal of parasitology *51*, 703-710. 10.3347/kjp.2013.51.6.703.

Piratae, S., Tesana, S., Jones, M.K., Brindley, P.J., Loukas, A., Lovas, E., Eursitthichai, V., Sripa, B., Thanasuwan, S., and Laha, T. (2012). Molecular characterization of a tetraspanin from the human liver fluke, Opisthorchis viverrini. PLoS Negl Trop Dis *6*, e1939. 10.1371/journal.pntd.0001939.

Rabacal, W., Schweitzer, F., Rayens, E., Tarantelli, R., Whang, P., Jimenez, V.C., Outwater, J.A., and Norris, K.A. (2019). Statin treatment prevents the development of pulmonary arterial hypertension in a nonhuman primate model of HIV-associated PAH. Scientific Reports *9*, 19832. 10.1038/s41598-019-55301-9.

Ran, F.A., Hsu, P.D., Wright, J., Agarwala, V., Scott, D.A., and Zhang, F. (2013). Genome engineering using the CRISPR-Cas9 system. Nature Protocols *8*, 2281-2308. 10.1038/nprot.2013.143.

Sato, Y., Sasaki, M., Harada, K., Aishima, S., Fukusato, T., Ojima, H., Kanai, Y., Kage, M., Nakanuma, Y., and Tsubouchi, H. (2014). Pathological diagnosis of flat epithelial lesions of the biliary tract with emphasis on biliary intraepithelial neoplasia. J Gastroenterol *49*, 64-72. 10.1007/s00535-013-0810-5.

Schmittgen, T.D., and Livak, K.J. (2008). Analyzing real-time PCR data by the comparative CT method. Nature Protocols *3*, 1101-1108. 10.1038/nprot.2008.73.

Shimonishi, T., Sasaki, M., and Nakanuma, Y. (2000). Precancerous lesions of intrahepatic cholangiocarcinoma. J Hepatobiliary Pancreat Surg *7*, 542-550. 10.1007/s005340070002.

Smout, M.J., Laha, T., Mulvenna, J., Sripa, B., Suttiprapa, S., Jones, A., Brindley, P.J., and Loukas, A. (2009). A granulin-like growth factor secreted by the carcinogenic liver fluke, Opisthorchis viverrini, promotes proliferation of host cells. PLoS Pathog *5*, e1000611. 10.1371/journal.ppat.1000611.

Smout, M.J., Sotillo, J., Laha, T., Papatpremsiri, A., Rinaldi, G., Pimenta, R.N., Chan, L.Y., Johnson, M.S., Turnbull, L., Whitchurch, C.B., et al. (2015). Carcinogenic Parasite Secretes Growth Factor That Accelerates Wound Healing and Potentially Promotes Neoplasia. PLoS Pathog *11*, e1005209. 10.1371/journal.ppat.1005209.

Sripa, B., Brindley, P.J., Mulvenna, J., Laha, T., Smout, M.J., Mairiang, E., Bethony, J.M., and Loukas, A. (2012). The tumorigenic liver fluke Opisthorchis viverrini--multiple pathways to cancer. Trends Parasitol *28*, 395-407. 10.1016/j.pt.2012.07.006.

Sripa, B., Kaewkes, S., Sithithaworn, P., Mairiang, E., Laha, T., Smout, M., Pairojkul, C., Bhudhisawasdi, V., Tesana, S., Thinkamrop, B., et al. (2007). Liver fluke induces cholangiocarcinoma. PLoS Med *4*, e201. 10.1371/journal.pmed.0040201.

Sripa, B., Tangkawattana, S., Laha, T., Kaewkes, S., Mallory, F.F., Smith, J.F., and Wilcox, B.A. (2015). Toward integrated opisthorchiasis control in northeast Thailand: the Lawa project. Acta Trop *141*, 361-367. 10.1016/j.actatropica.2014.07.017.

Sripa, B., Tangkawattana, S., and Sangnikul, T. (2017). The Lawa model: A sustainable, integrated opisthorchiasis control program using the EcoHealth approach in the Lawa Lake region of Thailand. Parasitol Int *66*, 346-354. 10.1016/j.parint.2016.11.013.

Sudsarn, P., Boonmars, T., Ruangjirachuporn, W., Namwat, N., Loilome, W., Sriraj, P., Aukkanimart, R., Nadchanan, W., and Jiraporn, S. (2016). Combination of Praziquantel and Aspirin Minimizes Liver Pathology of Hamster Opisthorchis viverrini Infection Associated Cholangiocarcinoma. Pathol Oncol Res *22*, 57-65. 10.1007/s12253-015-9967-y.

Sudsarn, P., Wongchalee, N., Boonmars, T., Laummaunwai, P., Chamgramol, Y., Pairojkul, C., Juasook, A., and Boonjaraspinyo, S. (2014). Sex differences in opisthorchiosis and the development of cholangiocarcinoma in Syrian hamster model. Parasitol Res *113*, 829-835. 10.1007/s00436-013-3713-8.

Surget, S., Khoury, M.P., and Bourdon, J.C. (2013). Uncovering the role of p53 splice variants in human malignancy: a clinical perspective. Onco Targets Ther *7*, 57-68. 10.2147/ott.S53876.

Suyapoh, W., Tangkawattana, S., Suttiprapa, S., Punyapornwithaya, V., Tangkawattana, P., and Sripa, B. (2021). Synergistic effects of cagA+ Helicobacter pylori co-infected with Opisthorchis viverrini on hepatobiliary pathology in hamsters. Acta Tropica *213*, 105740. https://doi.org/10.1016/j.actatropica.2020.105740.

Thamavit, W., Kongkanuntn, R., Tiwawech, D., and Moore, M.A. (1987). Level of Opisthorchis infestation and carcinogen dose-dependence of cholangiocarcinoma induction in Syrian golden hamsters. Virchows Arch B Cell Pathol Incl Mol Pathol *54*, 52-58. 10.1007/bf02899196.

Thamavit, W., Pairojkul, C., Tiwawech, D., Shirai, T., and Ito, N. (1994). Strong promoting effect of Opisthorchis viverrini infection on dimethylnitrosamine-initiated hamster liver. Cancer letters *78*, 121-125. 10.1016/0304-3835(94)90040-x.

Young, N.D., Nagarajan, N., Lin, S.J., Korhonen, P.K., Jex, A.R., Hall, R.S., Safavi-Hemami, H., Kaewkong, W., Bertrand, D., Gao, S., et al. (2014). The Opisthorchis viverrini genome provides insights into life in the bile duct. Nat Commun *5*, 4378. 10.1038/ncomms5378.

Zen, Y., Adsay, N.V., Bardadin, K., Colombari, R., Ferrell, L., Haga, H., Hong, S.M., Hytiroglou, P., Kloppel, G., Lauwers, G.Y., et al. (2007). Biliary intraepithelial neoplasia: an international interobserver agreement study and proposal for diagnostic criteria. Modern pathology : an official journal of the United States and Canadian Academy of Pathology, Inc *20*, 701-709. 10.1038/modpathol.3800788.

Figure legends

Figure 1. Experimental designs. Hamsters were infected with gene edited or control flukes for 14 weeks to assess the impact of CRISPR/Cas9 editing on fluke survival (panel **A**) or 24 weeks to assess the impact of CRISPR/Cas9 editing on pathogenesis including CCA **(B)**. Each experiment had three groups of hamsters infected with flukes treated with CRISPR/Cas9 plasmids targeting either *Ov-grn-1* **(**red**:** *ΔOv-grn-1)*, *Ov-tsp-2* (green**:** *ΔOv-tsp-2*), or a scrambled control (blue: SCR**)** designed to not match any *O. viverrini* sequence. For both experiments two hundred newly excysted juveniles (NEJ) per cuvette were transfected with 10 µg of CRISPR-Cas9 plasmid via electroporation **(**lightning bolt**)**. Each hamster was infected with 100 NEJs by stomach intubation After 2 weeks, the hamsters were supplied 12**.**5 ppm dimethyl nitrosamine (DMN) in drinking water for 10 weeks to accelerate carcinogenesis**.** In experiment 1, eggs per gram of feces **(**EPG**)** was determined at 10 and 12 weeks and the hamsters euthanized at week 14 of infection. In experiment 2, EPG was assessed at week 23 followed by euthanasia at week 24. Transcript levels in edited NEJs of *Ov-grn-1* **(B)** and *Ov-tsp-2* **(C)** were assessed by qPCR. To monitor programmed gene knockout, the gene transcript levels in 200 pooled NEJs were determined with 2-4 biological qPCR replicates and were plotted relative to 100% SCR control transcript levels. Each targeted gene shows significant transcript reduction in the relevant group, while the non-targeted gene shows no significant change to the SCR transcript level. Comparing each group with one-way ANOVA with Holm-Sidak multiple comparison against SCR control**:** *ns* = not significant; *, $P \leq 0.05$; ***,** $P \leq 0.01$; *ΔOv-grn-1* vs *ΔOv-tsp-2***,** ##, $P \leq 0.01$.

Figure 2. Liver fluke burden and levels of gene transcription. Fluke fecundity, adult fluke numbers, and gene expression levels were determined at 10-14 weeks **(**experiment 1**)** with 100 gene edited NEJs per hamster, and from three hamsters per group**.** Number of eggs per gram of feces **(**EPG**)** from each hamster at weeks 10 and 12 (**A**) and fluke burden at week 14 **(B)** showing average **(**horizonal black line**)** and SEM bars**.** Each treatment group was compared against matched SCR control with 2-way ANOVA with Holm-Sidak multiple comparison**:** ns = not significant; ***,** $P \leq 0.01$; ****,** $P<0.001$, and against Δ*Ov-tsp-2:* # **,** $P \leq 0.05$**.** A total of 10-12 flukes per animal were processed for qPCR to determine gene transcript levels of *Ov-grn-1* **(C)**

and Ov-tsp-2 **(D)** and plotted as violin plots with each data point representing the transcript level of individual flukes relative to control flukes; median denoted by thick colored line and quartiles by the black line. The distribution was non-parametric and subsequently the two-tailed Mann-Whitney *t* test was used to compare transcript levels with those of the SCR control; ****,** $P \leq 0.01$; *****,** $P \leq 0.001$ for each gene.

Figure 3. Cholangiocarcinoma model, fecundity, and gene transcript and mutation rates. Eggs per gram of feces (EPG) was assessed at week 23 prior to euthanasia at week 24 (experiment 2). Panel **A** shows the EPG of the three groups of all hamsters. Violin plot denotes each animal's EPG with "x" symbols. Circle enclosed "x", (ⓧ), signifies animals with low EPG below 1,000 and square enclosed "x", (⊠), signifies animals with high EPG above 20,000. Solid colored lines indicate the median values and dashed black lines indicate the quartiles. **B** shows the same EPG with low/high animals removed, these "moderate EPG" animals had 1,000-20,000 EPG. The distribution was non-parametric and subsequently the Kruskal Wallis with Dunn's multiple comparison correction was used to compare EPG levels against SCR control: *, $P < 0.05$; ns = not significant. At week 24, hamsters were euthanized, 12-20 flukes collected from each group and transcript levels of *Ov-grn-1* **(C)** or *Ov-tsp-2* **(D)** determined. Violin plots are shown with each data point representing the transcript level for individual flukes relative to control flukes. The thick solid line is the median and the dashed black lines are the inter-quartile ranges. **C, D**, Mann-Whitney non-parametric *t*-test comparing transcript levels against SCR control for each gene: ns, not significant; ******,** $P \leq 0.0001$.

Figure 4. Gene mutation rates among liver flukes. Panel **A,** CRISPR/Cas9 gene editing is highly effective in only some flukes. Insertion/deletion (indel) mutation rate ~60 base pairs either side of the CRISPR/Cas9 double stranded break from CRISPResso2 analysis of NGS data, plotted as a violin plot. SCR NEJs and adult flukes are each from a single pooled sample, while *ΔOv-grn-1* NEJs are from two biological replicate pooled samples, and *ΔOv-grn-1* adult flukes from 13 individual adult flukes. The highly edited flukes are denoted as $_{H}$*ΔOv-grn-1*, flukes with low editing denoted as $_{L}$*ΔOv-grn-1*, and flukes with medium level editing denoted as $_{M}$*ΔOv-grn-1*. One sample *t* test for either NEJs or adults comparing *ΔOv-grn-1* and SCR: * = $P<0.05$; ** = $P<0.01$. The thick solid line is the median and the inter-quartiles are black dashed lines. Note the

broken Y-axis with a magnified lower portion to highlight the near zero values. **B.** Adult fluke indel mutation rate is inversely correlated with transcript level. The indel and transcript levels plotted for each individual *ΔOv-grn-1* fluke (red circles, combining data from Figures 3C and 4A) showed that the highly mutated (>50%, $_{H}$*ΔOv-grn-1*) flukes generally showed low (<11%) *Ov-grn-1* transcript levels, while low edited flukes ($_{L}$*ΔOv-grn-1*) generally showed higher transcript levels. Highly significant two-tailed non-parametric correlation determined by Spearman co-efficient, $r_s = -0.74$ (**, $P \leq 0.01$). The negative linear correlation (slope -0.77) is shown as a red line with shaded 95% confidence intervals (r^2=0.62). For context, the SCR indel% are plotted against the transcript median (blue triangle) with interquartile range error bars. **C.** *ΔOv-grn-1* indel location and frequency within adult worms. The NGS sequencing reveals distinct Indel patterns in 12/13 flukes determined with CRISPResso2. Shown as a multivariate bubble plot, the amplicon base pair open reading frame (ORF position) was plotted against the average indel length. The size of the bubbles (1-11) reflects how many of 13 adult flukes recorded a matching indel. The CRISPR/Cas9 cut site between nt 19/20 is marked with "cut". To aid visualization the Adult deletions (blue) and insertions (red) have been nudged up/down on the y-axis +/-0.1. The NEJ deletions (yellow) are shown from one pooled sample and no NEJ insertions were seen. Position -9 is highlighted with a vertical dotted line and the black horizontal square bracket (└─┘) highlights the pre-ORF Indel cluster at positions -1 to -10. The genetic sequence in proximity to this cluster is shown below the x-axis and the ORF initiator methionine sequence (ATG) is highlighted in red. The majority of Indels were 1-4 nt, but a single fluke was recorded with 13 large deletions of 31-62 bp (gray dashed oval). **D.** When successful *Ov-grn-1* gene editing was seen, the majority occurred at a single location. The graph plots the Indel position against the frequency with each *ΔOv-grn-1* adult Indel shown as individual marks: highly edited ($_{H}$*ΔOv-grn-1, green* +); medium edited ($_{M}$*ΔOv-grn-1*, purple +); low edited ($_{L}$*ΔOv-grn-1*, red x). Pooled samples are shown as *ΔOv-grn-1* NEJs (orange circle), SCR NEJs (light blue triangle), and SCR adults (dark blue triangle). A vertical dotted line highlights the hotspot at nt -9 that comprised 98.5-99.9% of the observed indel% for successfully edited *ΔOv-grn-1* flukes and NEJs. No $_{L}$*ΔOv-grn-1* adults, SCR NEJs or adults showed editing at this position. This hotspot is within the pre-ORF indel cluster at positions -1 to -10 (black horizontal square bracket: └─┘). Other locations with frequently noted indels are labeled with the position number and corresponding nucleotide letter.

Figure 5. Hepatobiliary disease burden in liver fluke infection associated cholangiocarcinoma. Livers were harvested and a component of each lobe was prepared for sectioning or used for harvesting flukes for subsequent analysis (Fig. 1, Experiment 2). Gross appearance and histopathological results from cholangiocarcinoma (Kitadokoro *et al.*) induction using dimethyl nitrosamine (DMN) and gene edited newly excysted juveniles (NEJ) infection. Multiple CCA nodules in the hamster liver presented in both diaphragmatic **(A)** and visceral surfaces **(B)**. H&E stained histology slide highlighting foci of moderate dysplasia **(C).** This image consists of bile ducts (blue #) encircled by dysplastic biliary epithelium (yellow arrow) surrounded by fibrosis (fb) with hepatocytes (h) to the left. Histological H&E stained images of CCA from each of the hamster groups: SCR **(D),** *ΔOv-grn-1* **(E),** and *ΔOv-tsp-2* **(F)**. Inflammation marked with (green asterisk *), cholangiocarcinoma labelled with CCA and other labels are as detailed in panel C. Euthanized hamster livers were sectioned and examined for degree of pathogenesis. **G.** Assessment of the highest degree of pathological lesions or CCA development present in entire liver sections of all animals was conducted by two experienced veterinary pathologists using blinded H&E stained slides. The lesions increased in severity from none (grey) to high grade CCA (red) spanning multiple liver lobes. **H**. The gross overall liver pathology with only "moderate EPG" phenotype hamsters. If no animal was noted in a category, a thin band of color is shown. **I.** EPG from individual hamsters plotted against the pathology status on a scale of zero (0, no lesion) to 6 (high CCA) scale. The cutoffs for 1,000 to 20,000 "moderate EPG" data are highlighted with vertical dashed lines. Data points were nudged ± 0.1 on the Y-axis to mitigate e the display of overlapping points. Hamsters with EPG >1,000 did not show significant correlation between EPG and pathogenesis (two-tailed non-parametric Spearman correlation, $P>0.05$).

Figure 6. Attenuated hepatic fibrosis during infection with Δ*Ov-grn-1* gene edited liver flukes. **A.** Representative images of hepatic fibrosis stained by Picro-Sirius Red with CRISPR-Cas9 edited *O. viverrini* from the 24-week CCA model. Fibrosis is denoted as pink/red thick bands around the bile ducts (periductal fibrosis, fb) and expands from each portal triad with fibrous septa. OV = *Opisthorchis viverrini* fluke, H = hepatocytes, BD = bile duct, BE = biliary epithelium. **B**. Global liver fibrosis plotted as a violin plot. Livers were scored for pathogenic

fibrosis with an Ishak Stage Grading scale and plotted on a violin graph that spans from zero (no fibrosis) to six (cirrhosis). **C.** Fibrosis proximal to flukes plotted as a violin plot. Automated ImageJ fibrosis analyzer software evaluation of the percentage of collagen deposition in images surrounding fluke-containing bile ducts. Panels B+C: median shown as thick colored line and dashed black lines mark the inter-quartile ranges. Comparing groups with Kruskal-Wallis test with Dunn's multiple comparisons against SCR: *ns* = not significant; **, $P \leq 0.05$; ***, $P \leq 0.0001$, and against *ΔOv-tsp-2* group: #, $P \leq 0.05$; ##, $P \leq 0.01$.

Figure 7. Reduced cholangiocyte proliferation and p53 expression during infection with Δ*Ov-grn-1 O. viverrini*. Representative images of proliferating biliary cells that incorporated BrdU from liver samples proximal to flukes in SCR, Δ*Ov-grn-1* and Δ*Ov-tsp-2* groups **(A)**. The boxed region in the upper image is magnified in the lower panel. The brown arrow highlights the positive BrdU-stained nuclei in each image and the blue arrow highlights a negative bile duct cell that did not incorporate BrdU. Violin graphs of BrdU index measured from cholangiocytes in bile ducts containing a fluke **(B)**. Representative micrograph of p53 immunohistochemistry of biliary epithelium of DMN-exposed hamsters infected with gene edited liver flukes **(C).** Anti-p53 antibody stained nuclei brown (brown arrows); unstained negative cells indicated using blue arrows. Black dashed box in upper wide-angle image is magnified in the lower image to aid visualization. Violin plot of p53 positive cholangiocytes as a percentage **(D).** Where available, 500 to 800 cells were scored from sections of each of the left, middle, and right lobes of the liver of hamsters with "moderate EPG", and marked by a grey "x". Note: only 300-500 cholangiocytes were available for p53 assessment in some samples; three Δ*Ov-grn-1* lobes and three Δ*Ov-tsp-2* lobes. In these cases, all cholangiocytes were counted and marked with ⓧ. Panels A+C: OV = *Opisthorchis viverrini* fluke, H = hepatocytes, BD = bile duct, BE = biliary epithelium. Panels B, D: non-parametric Kruskal-Wallis test with Dunn's multiple comparison correction compared against SCR: ns = not significant; **, $P \leq 0.01$; ****, $P \leq 0.0001$, or against *ΔOv-tsp-2*: *ns*, not significant; #, $P \leq 0.05$; #, $P \leq 0.01$. Thick colored lines signify the median and the dashed black lines mark the inter-quartile ranges.

1139

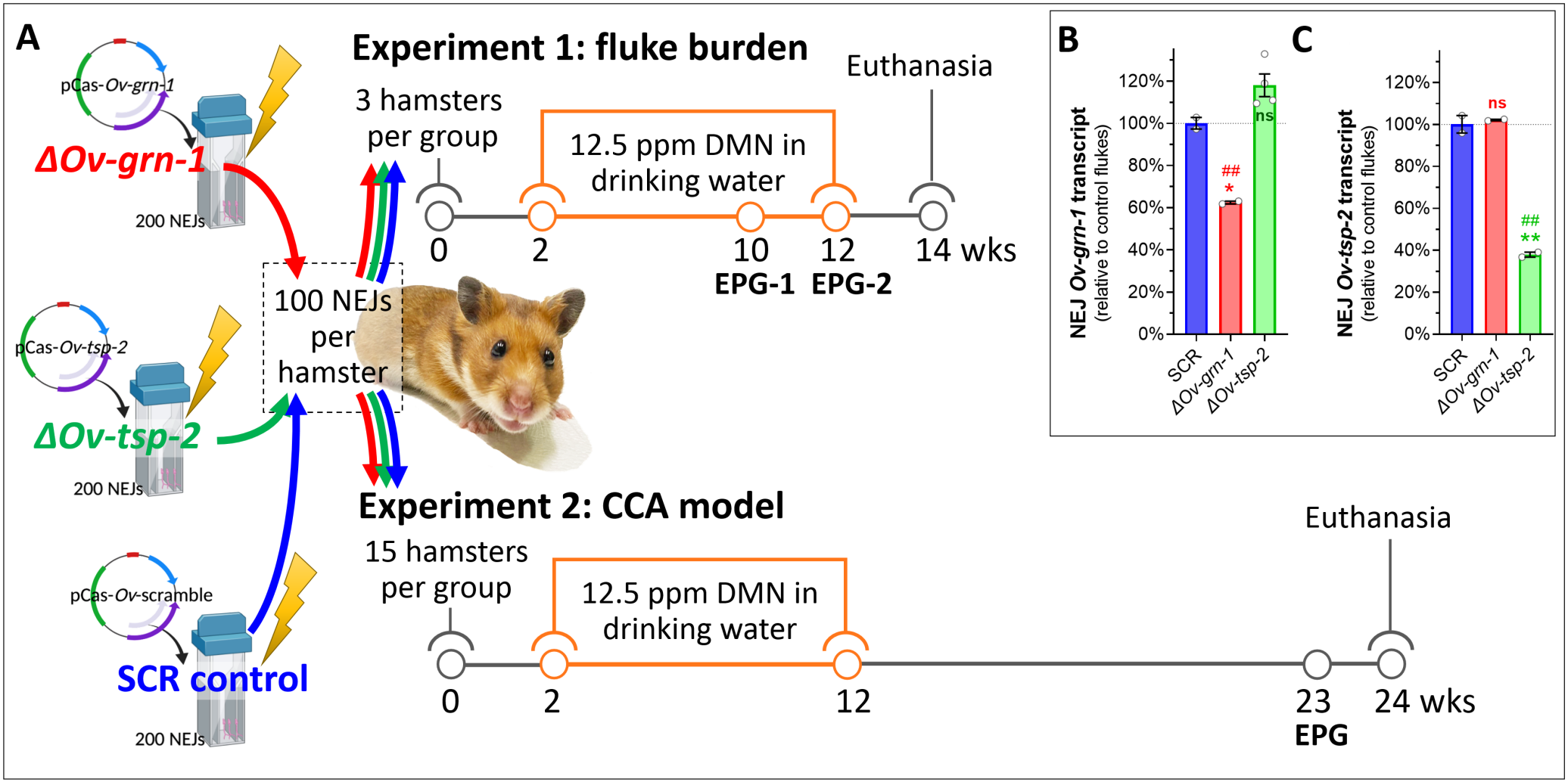
A
pCas-Ov-grn-1
ΔOv-grn-1
200 NEJs
pCas-Ov-tsp-2
ΔOv-tsp-2
200 NEJs
pCas-Ov-scramble
SCR control
200 NEJs
100 NEJs per hamster
Experiment 1: fluke burden
3 hamsters per group
12.5 ppm DMN in drinking water
Euthanasia
0
2
10
12
14 wks
EPG-1
EPG-2
Experiment 2: CCA model
15 hamsters per group
12.5 ppm DMN in drinking water
Euthanasia
0
2
12
23
24 wks
EPG
B
NEJ Ov-grn-1 transcript
(relative to control flukes)
120%
100%
80%
60%
40%
20%
0%
##
*
ns
SCR
ΔOv-grn-1
ΔOv-tsp-2
C
NEJ Ov-tsp-2 transcript
(relative to control flukes)
ns
##
**

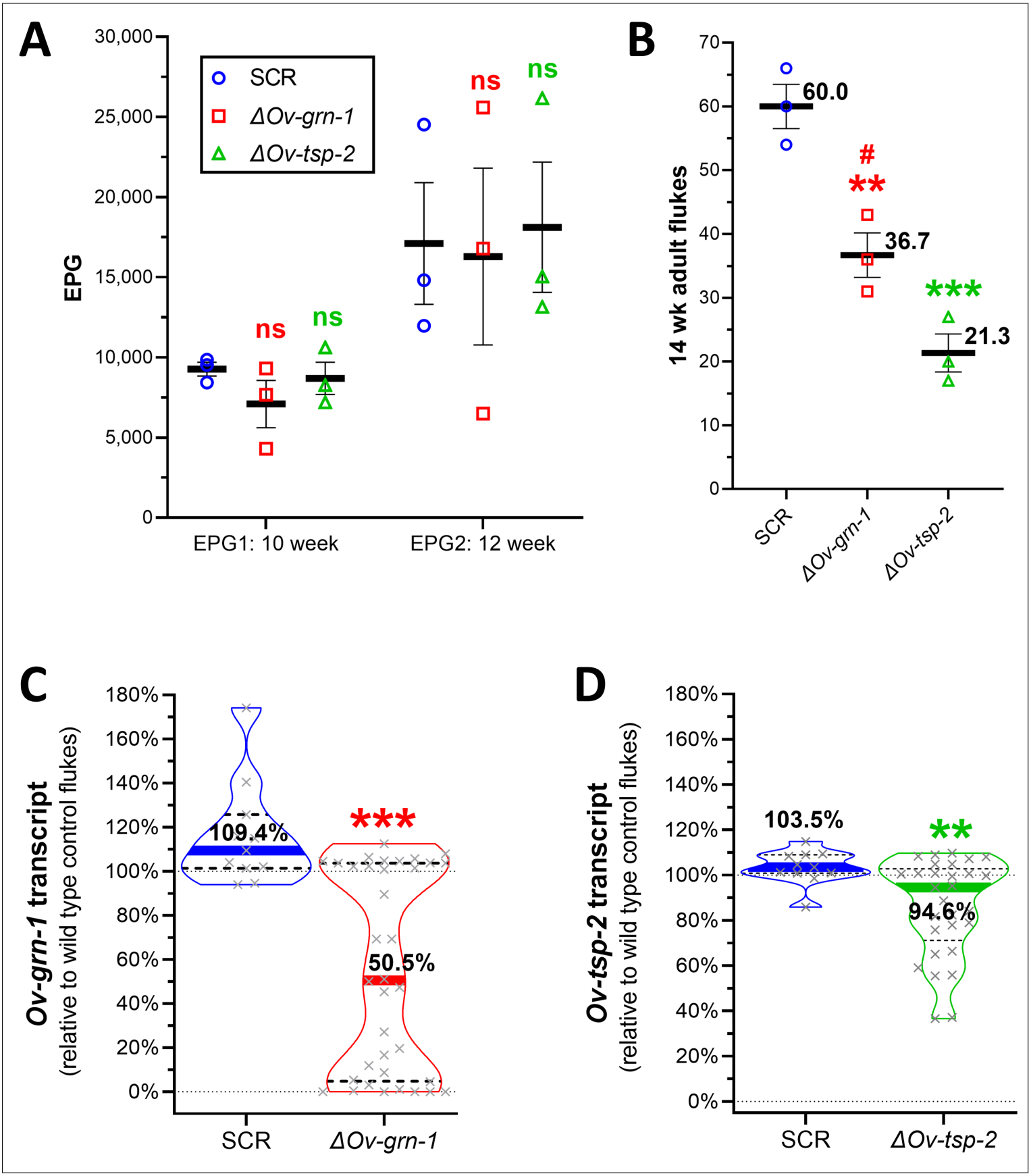
A
30,000
25,000
20,000
15,000
10,000
5,000
0
EPG
SCR
ΔOv-grn-1
ΔOv-tsp-2
ns
ns
ns
ns
EPG1: 10 week
EPG2: 12 week
B
70
60
50
40
30
20
10
0
14 wk adult flukes
60.0
#
**
36.7
***
21.3
SCR
ΔOv-grn-1
ΔOv-tsp-2
C
180%
160%
140%
120%
100%
80%
60%
40%
20%
0%
Ov-grn-1 transcript
(relative to wild type control flukes)
109.4%
***
50.5%
SCR
ΔOv-grn-1
D
180%
160%
140%
120%
100%
80%
60%
40%
20%
0%
Ov-tsp-2 transcript
(relative to wild type control flukes)
103.5%
**
94.6%
SCR
ΔOv-tsp-2

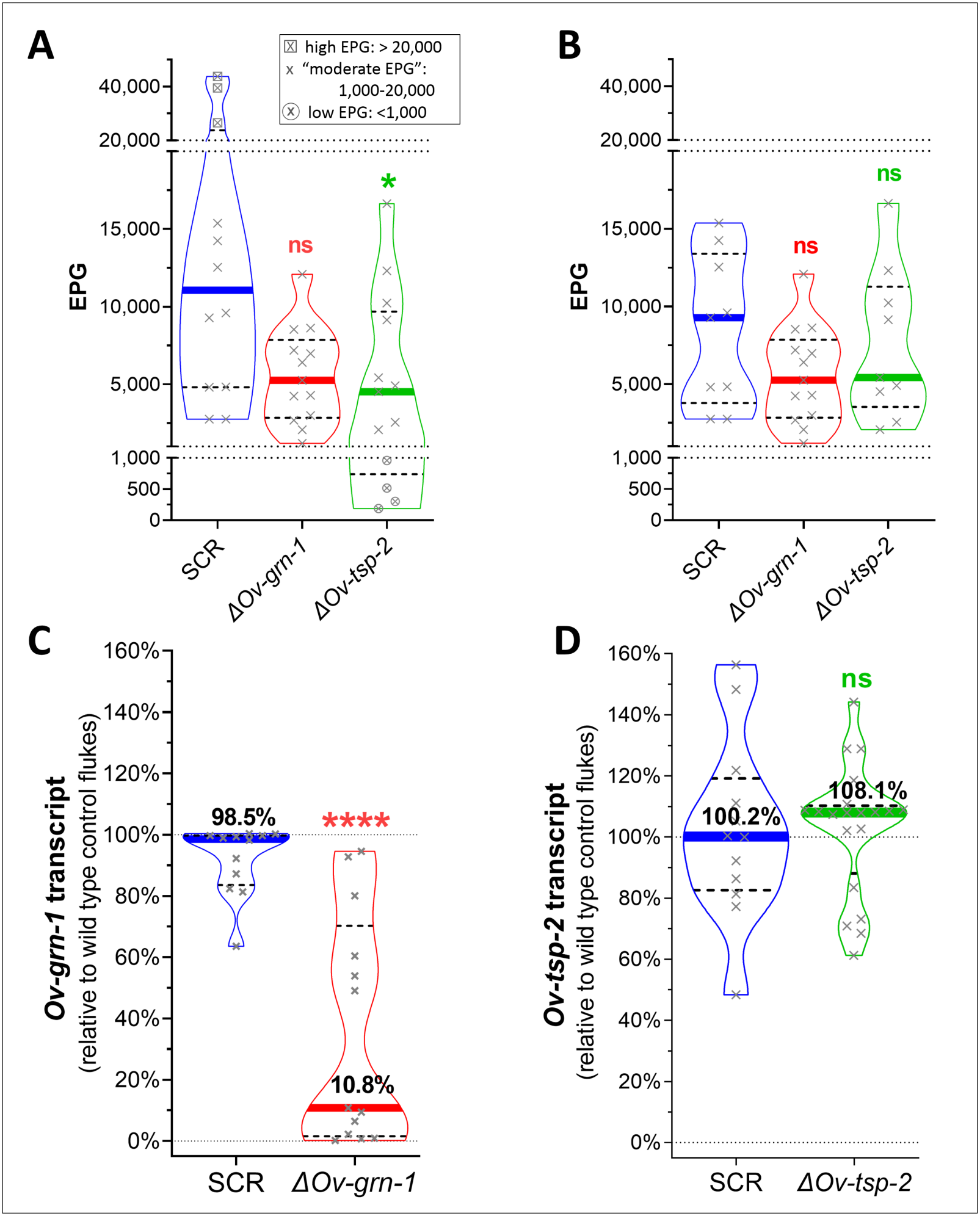
A
high EPG: > 20,000
"moderate EPG": 1,000-20,000
low EPG: <1,000
EPG
40,000
20,000
15,000
10,000
5,000
1,000
500
0
ns
*
SCR
ΔOv-grn-1
ΔOv-tsp-2
B
EPG
ns
ns
SCR
ΔOv-grn-1
ΔOv-tsp-2
C
Ov-grn-1 transcript
(relative to wild type control flukes)
160%
140%
120%
100%
80%
60%
40%
20%
0%
98.5%
****
10.8%
SCR
ΔOv-grn-1
D
Ov-tsp-2 transcript
(relative to wild type control flukes)
ns
100.2%
108.1%
SCR
ΔOv-tsp-2

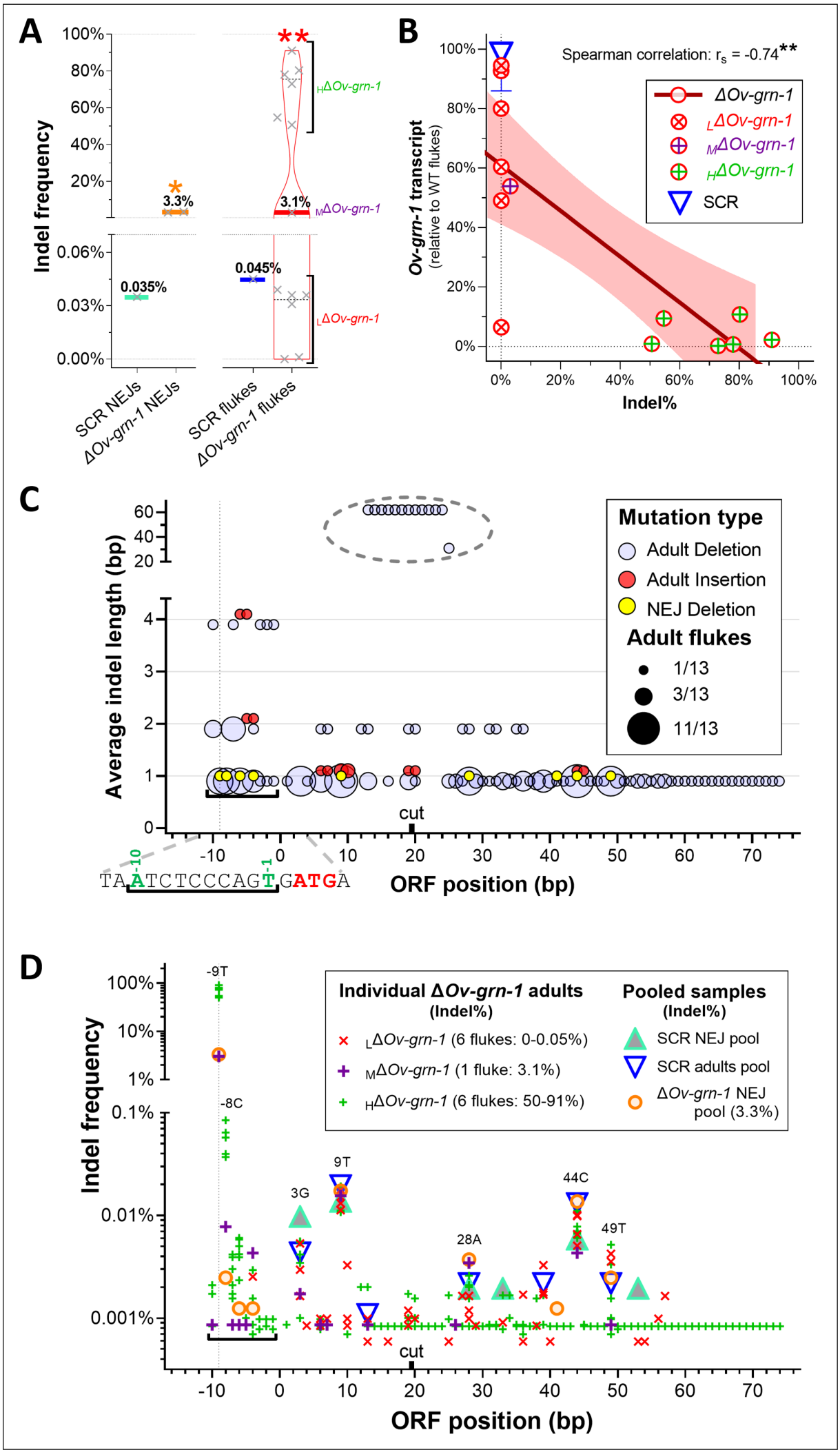
A
Indel frequency
100%
80%
60%
40%
20%
0.06%
0.03%
0.00%
3.3%
0.035%
0.045%
3.1%
**
*
HΔOv-grn-1
MΔOv-grn-1
LΔOv-grn-1
SCR NEJs
ΔOv-grn-1 NEJs
SCR flukes
ΔOv-grn-1 flukes
B
Spearman correlation: rs = -0.74**
Ov-grn-1 transcript
(relative to WT flukes)
Indel%
ΔOv-grn-1
LΔOv-grn-1
MΔOv-grn-1
HΔOv-grn-1
SCR
C
Average indel length (bp)
ORF position (bp)
cut
Mutation type
Adult Deletion
Adult Insertion
NEJ Deletion
Adult flukes
1/13
3/13
11/13
-10
-1
TAATCTCCCAGTGATGA
D
Indel frequency
ORF position (bp)
cut
-9T
-8C
3G
9T
28A
44C
49T
Individual ΔOv-grn-1 adults
(Indel%)
LΔOv-grn-1 (6 flukes: 0-0.05%)
MΔOv-grn-1 (1 fluke: 3.1%)
HΔOv-grn-1 (6 flukes: 50-91%)
Pooled samples
(Indel%)
SCR NEJ pool
SCR adults pool
ΔOv-grn-1 NEJ pool (3.3%)

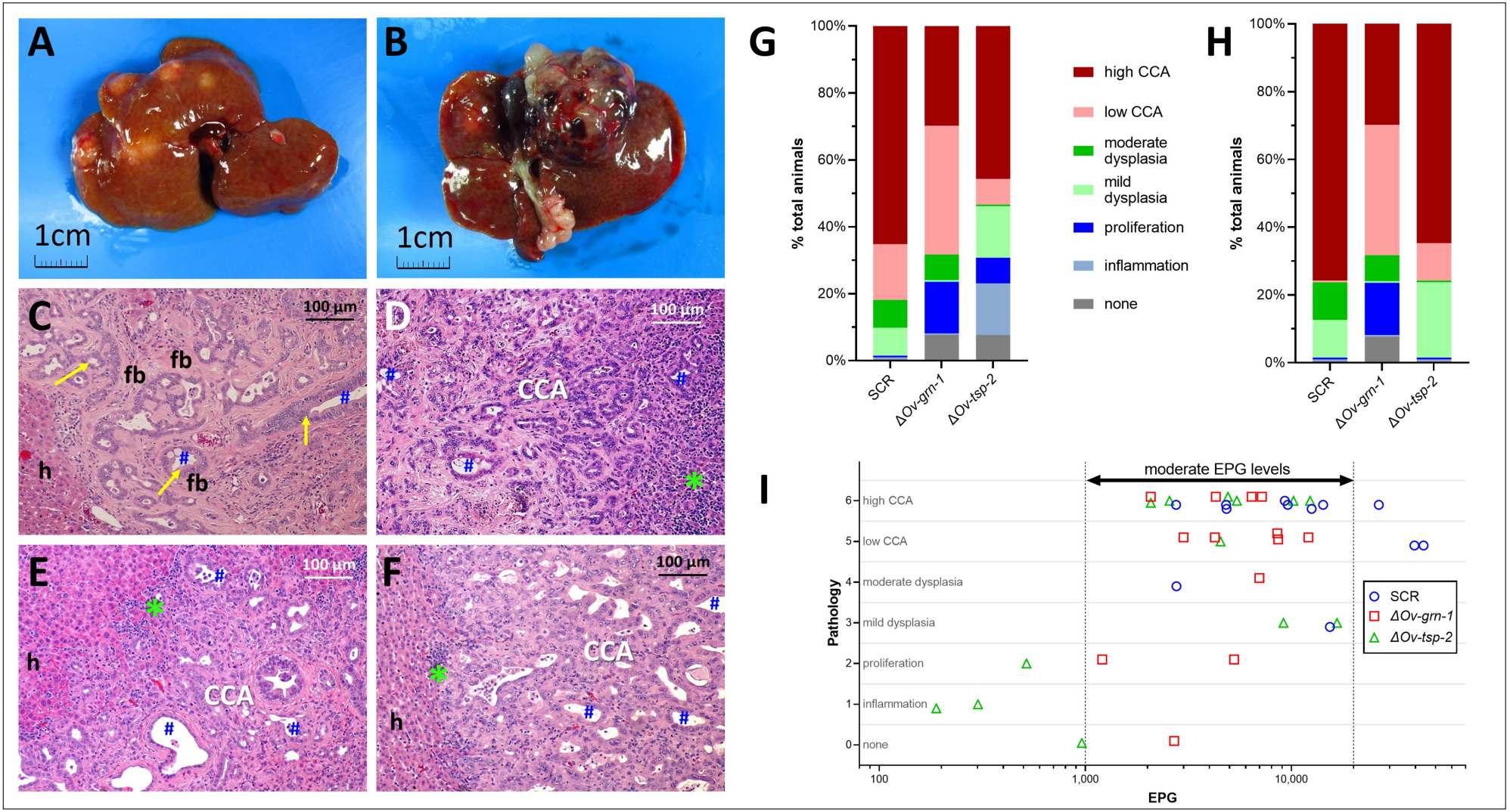
A
1cm
B
1cm
C
100 µm
fb
fb
fb
h
D
100 µm
CCA
E
100 µm
h
CCA
F
100 µm
CCA
h
G
% total animals
100%
80%
60%
40%
20%
0%
SCR
ΔOv-grn-1
ΔOv-tsp-2
high CCA
low CCA
moderate dysplasia
mild dysplasia
proliferation
inflammation
none
H
% total animals
100%
80%
60%
40%
20%
0%
SCR
ΔOv-grn-1
ΔOv-tsp-2
I
moderate EPG levels
Pathology
6 high CCA
5 low CCA
4 moderate dysplasia
3 mild dysplasia
2 proliferation
1 inflammation
0 none
100
1,000
10,000
EPG
SCR
ΔOv-grn-1
ΔOv-tsp-2

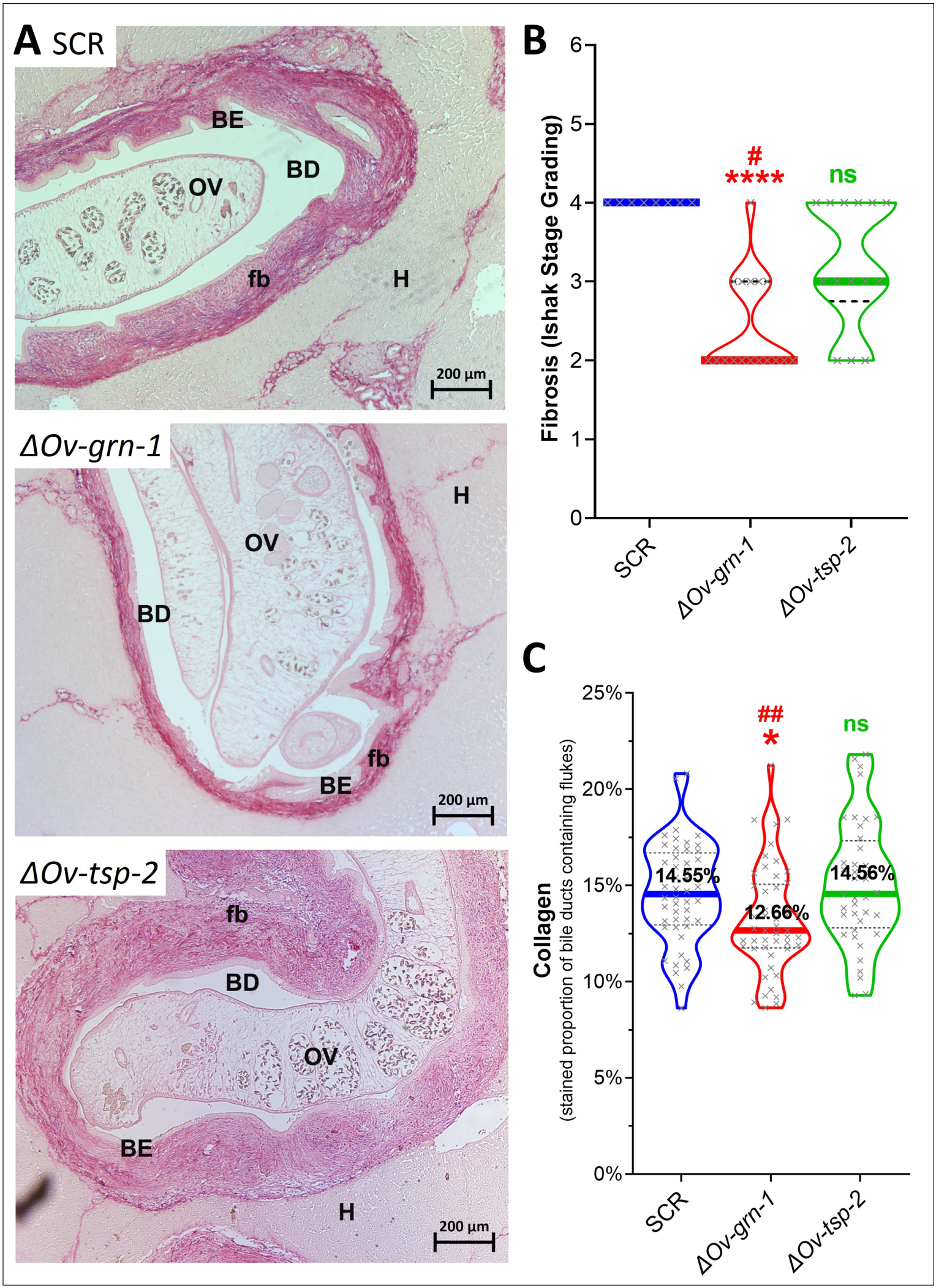
A SCR
BE
BD
OV
fb
H
200 µm
ΔOv-grn-1
H
OV
BD
fb
BE
200 µm
ΔOv-tsp-2
fb
BD
OV
BE
H
200 µm
B
Fibrosis (Ishak Stage Grading)
0
1
2
3
4
5
6
#
****
ns
SCR
ΔOv-grn-1
ΔOv-tsp-2
C
Collagen
(stained proportion of bile ducts containing flukes)
0%
5%
10%
15%
20%
25%
##
*
ns
14.55%
12.66%
14.56%
SCR
ΔOv-grn-1
ΔOv-tsp-2

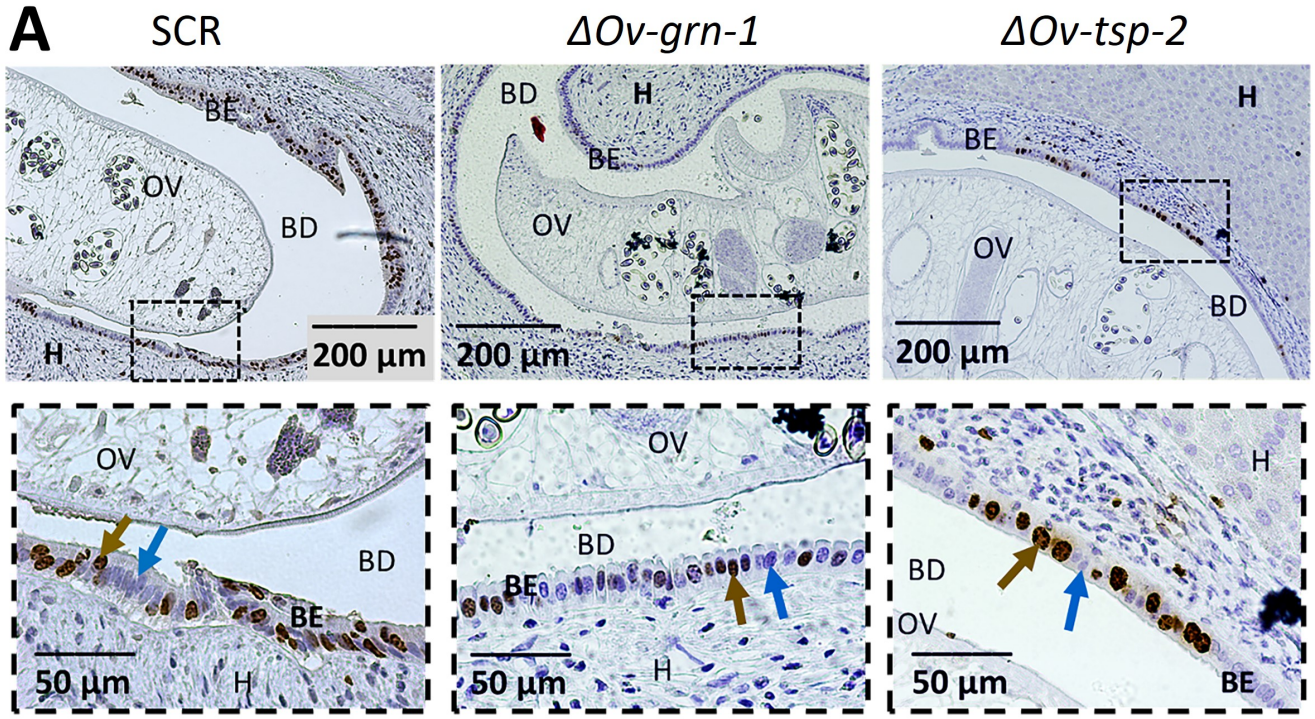
A
SCR
ΔOv-grn-1
ΔOv-tsp-2
BE
OV
BD
H
200 µm
50 µm

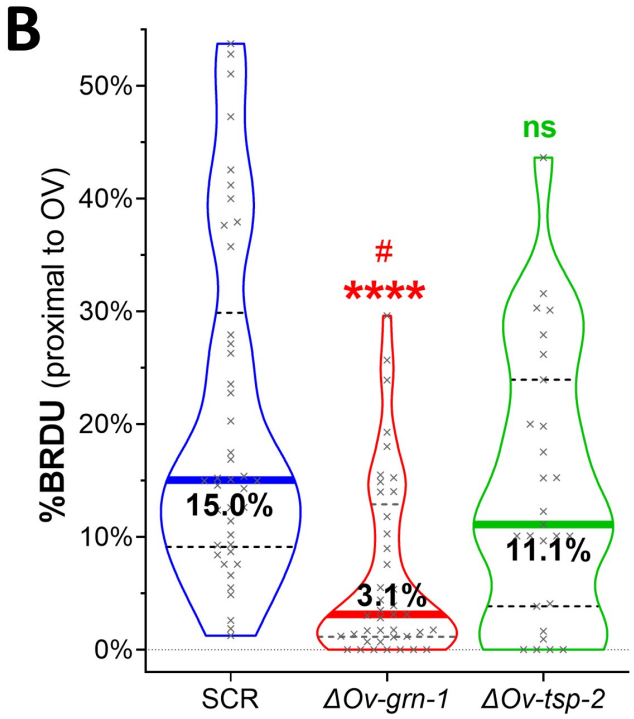
B
%BRDU (proximal to OV)
50%
40%
30%
20%
10%
0%
15.0%
3.1%
11.1%
#
****
ns
SCR
ΔOv-grn-1
ΔOv-tsp-2

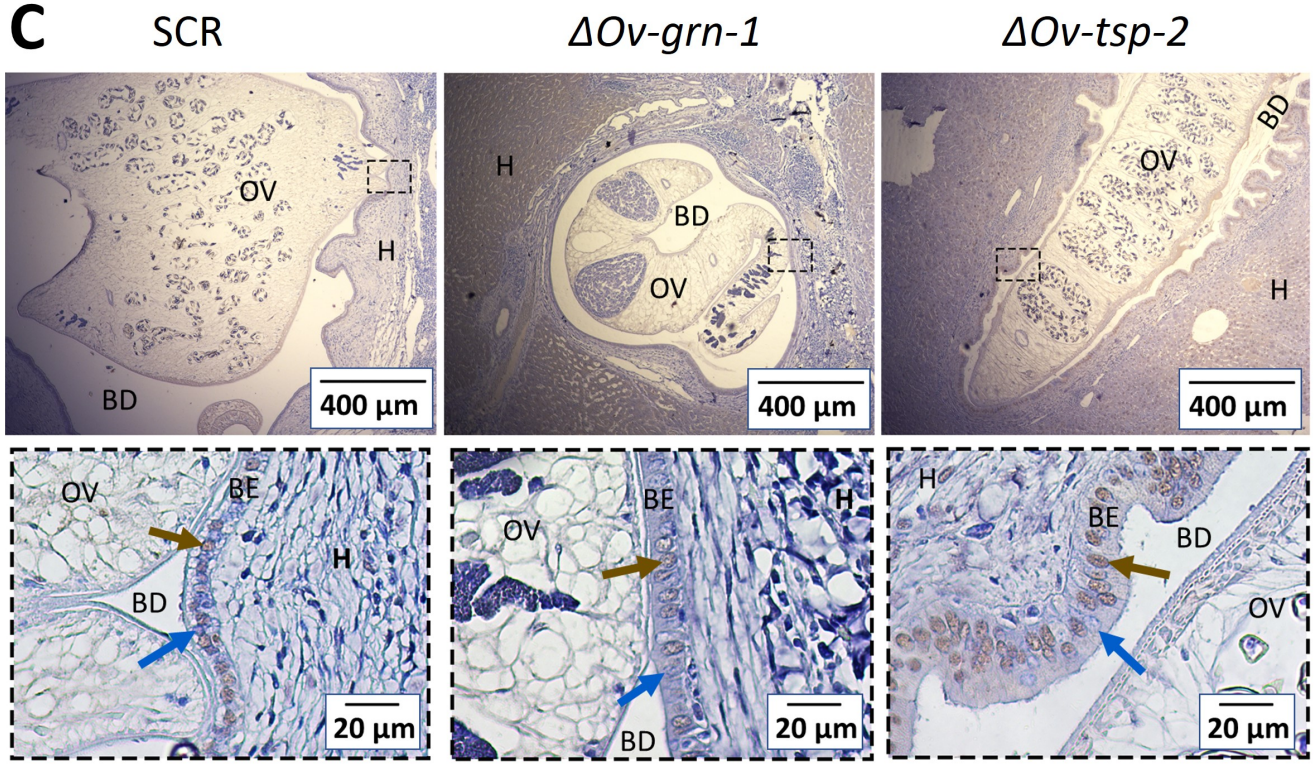
C
SCR
ΔOv-grn-1
ΔOv-tsp-2
OV
BD
H
BE
400 µm
20 µm

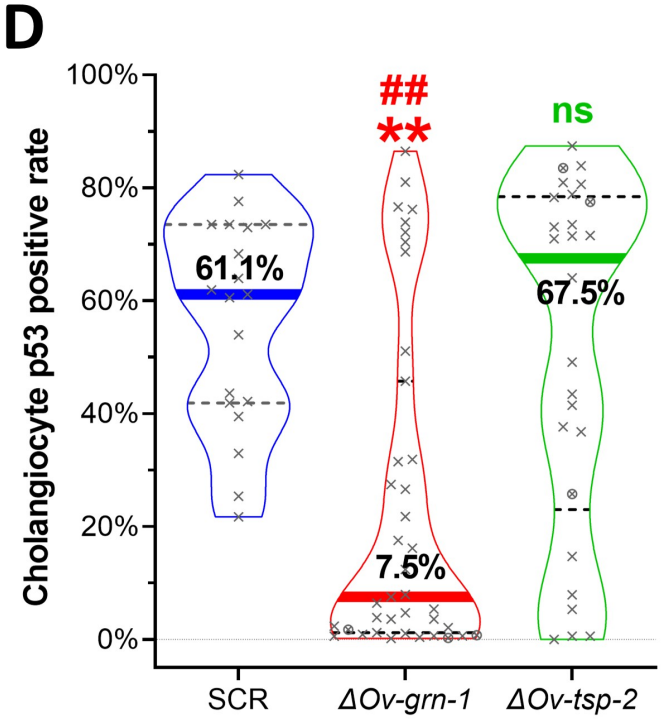
D
Cholangiocyte p53 positive rate
100%
80%
60%
40%
20%
0%
61.1%
7.5%
67.5%
##
**
ns
SCR
ΔOv-grn-1
ΔOv-tsp-2